DANMARKS OG GRØNLANDS GEOLOGISKE UNDERSØGELSE RAPPORT 2012/122

Magnetotelluric investigation of the Tønder area, Denmark

ALTKUL Project Report Part 2

T. M. Rasmussen, L.B. Pedersen, C. Shan & L. Thorning

(1 DVD included)

GEOLOGICAL SURVEY OF DENMARK AND GREENLAND
DANISH MINISTRY OF CLIMATE, ENERGY AND BUILDING

G E U S

DANMARKS OG GRØNLANDS GEOLOGISKE UNDERSØGELSE RAPPORT 2012/122

Magnetotelluric investigation of the Tønder area, Denmark

ALTKUL Project Report Part 2

T. M. Rasmussen, L.B. Pedersen, C. Shan & L. Thorning

(1 DVD included)

GEOLOGICAL SURVEY OF DENMARK AND GREENLAND
DANISH MINISTRY OF CLIMATE, ENERGY AND BUILDING

G E U S

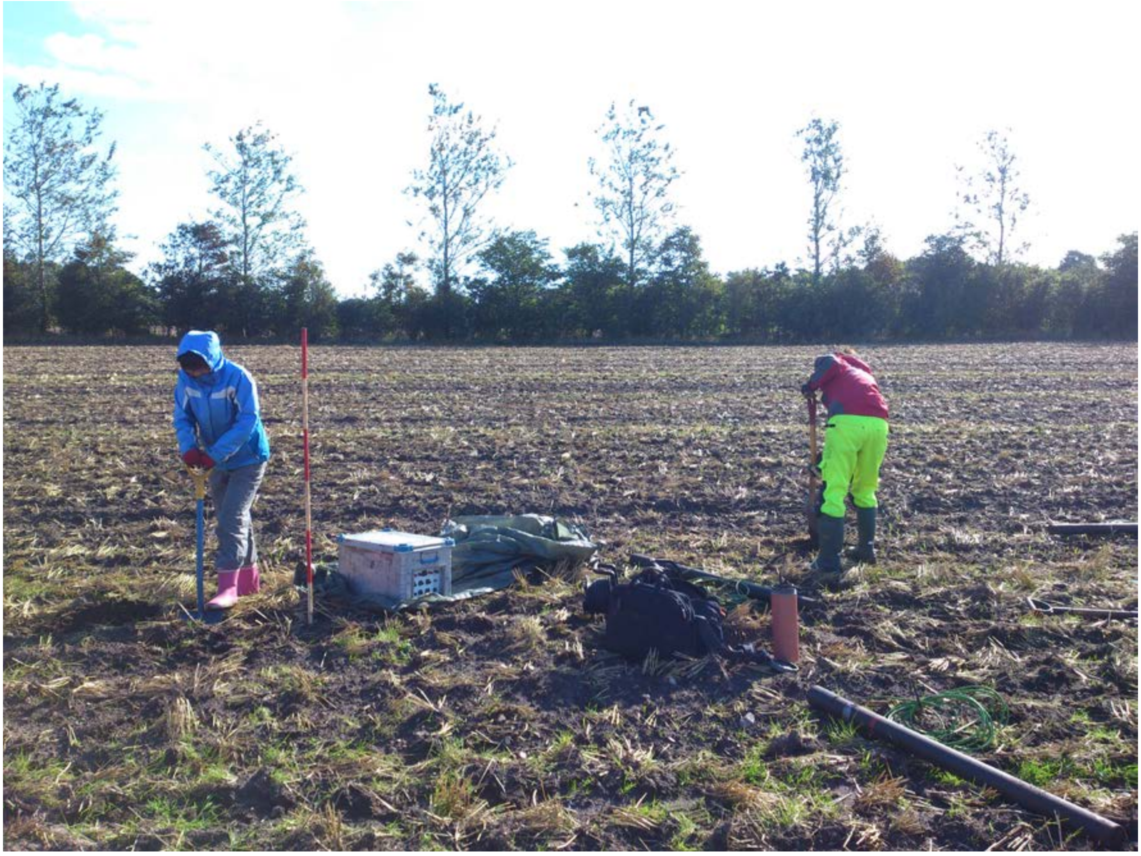

Contents

1. Executive summary

Project ALTKUL was commissioned by DONG E&P A/S and Nordsøfonden; the Danish Energy Agency followed the project closely.

The first part of the study has been reported in Rasmussen and Thorning (2012).The starting point of the study was a need for more knowledge on methods that could be used for hydrocarbon exploration in Danish onshore areas, as an alternative to seismic investigations, when these cannot be used for nature protecting reasons. DONG E&P A/S and Nordsøfonden approached GEUS, suggesting a study of seven different non-seismic methods. The Danish Energy Agency was interested in the subject and requested that an actual test of a method be carried out as a part of the project.

The optimum choice for a field test was an electromagnetic experiment with a galvanic controlled source (Rasmussen & Thorning, 2012). However, due to organisational issues and a limited timeframe of the project, the final choice of method for the field test was settled on using the magnetotelluric method (MT). Though MT does not utilise galvanic controlled sources, and hence does not serve as a tool for direct hydrocarbon exploration, MT has been used in the past in relation with hydrocarbon exploration onshore and has recently gained considerable interest in China. The application of MT in hydrocarbon exploration is directed towards mapping of conductive alteration zones surrounding reservoirs. The increase in conductivity is mainly a result of disseminated pyrite. The presence of pyrite may also imply that induced polarization phenomena are associated with the presence of reservoirs.

A contract was therefore entered into with Uppsala University for some initial tests of the magnetotelluric (MT) method. The test was carried out August 2012 in an area around Tønder, and is reported here as ALTKUL Project Report Part 2. In total 42 MT stations were measured in a 180 km^2 area. The digital data are enclosed with the report and hereby released to the public.

A 3D model of the electrical resistivity variations to a depth of 6 km constitutes, together with the actual measured data, the main results of part 2 of the ALTKUL project. The 3D model was derived from an unconstrained 3D inversion of the MT data. The MT data show that pronounced lateral resistivity variations exist at the depth of interest for hydrocarbons in the Tønder area. The resistivity variations clearly reflect the presence of salt tectonics in the survey area.

Another achievement from the test is the information on electromagnetic noise sources. The noise in the survey area was highly variable both spatially and with time. At some MT stations high quality data could be obtained. Other MT stations did not provide data of sufficiently quality to be included in the modelling.

Some tentative comments with respect to interpretation of the acquired MT data are provided. We do not enter into an in-depth interpretation of the data and derived model, but we conclude that the MT data provide valuable information on the regional variations of resistivity. A number of anomalies are evident which point to significant variations in resistivity laterally. Some inconsistencies in relation to information from deep wells are noted with respect to depth to stratigraphic units. This is particularly the case at the location of the Borg-1 well. The salt pillow around at Tønder is mapped well by the MT data.

The reporting of the test is structured as follows: after a short introduction (with some basic information on MT for readers unfamiliar with the method) follows the report by L.B. Pedersen and J. Shan, Uppsala University, which represents the core of the test. It includes a description of field work, noise conditions and data quality, data processing techniques and modelling. The report by Pedersen & Shan and accompanying appendix is included as chapter 3 in this GEUS report.

The last part of this report places the modelling results in context with geological information and other geophysical data publically available from the survey area. The purpose of this last part of the report is to provide information and considerations useful for further interpretation on the acquired new data. A section on the geology of the area is included with some key references and finally, another section includes displays of the model derived from the MT data from this study together with displays of other data. Resistivity logs from eight deep exploration wells within the survey areas are included for reference and comparison. The measured data are provided digitally with the intention that they can be integrated with other geological and geophysical data in future work.

2. Introduction to magnetotellurics

The purpose of this introduction is to provide readers unfamiliar with the MT method with the some basic concepts involved in the measuring, processing and modelling of MT data.

The MT method is based on induction of electromagnetic field in the ground by natural time varying electric sources. The sources are mainly the electrical current system in the ionosphere and electromagnetic fields associated with distant lightning phenomena. The two types differ with respect to frequency range involved. The ionosphere sources produce electromagnetic fields with frequencies mainly below 1 Hz, whereas the electromagnetic field caused by lightning has frequencies above 1 Hz. These two types of sources are utilised in magnetotellurics (MT) and audio-magnetotellurics (AMT), where simultaneous measurements at the ground surface of the time varying electric and magnetic fields are measured. The distinction between the two methods is essentially a matter of differences in frequency content, whereas the data collection, processing and interpretation techniques are nearly identical. Although the lightning phenomena are associated with electrical charge exchange (galvanic source) between the atmosphere and the earth locally, the energy utilised in the AMT methods is fully based on inductively generated current in the ground, where the electromagnetic wave has travelled - often several thousands of kilometres from mainly tropical regions - through the airspace before penetration into the ground.

The MT method was introduced in the 1950'ties by Cagniard (1953) and Tikhonov (1950, 1965). The method has undergone very significant improvements in terms of data quality of the measurements as well as possibilities for 2D inversion. Recently also 3D inversion has been made possible and the result presented in this report is the first reporting of 3D inversion of data acquired in Denmark. Chave & Jones (2012) provide a comprehensive treatment of theory and practice of the MT method. They mention that over 500 broad band (MT+AMT) systems from one manufacturer alone are in continuous use in China for oil and gas exploration onshore.

The method involves measurements of the electromagnetic field variations in time at the surface of the earth along two horizontal orthogonal directions. The electric field strength is of the order of a few micro Volts per metre. The amplitudes of the magnetic field variations are in the nTesla range. Induction coils are often used for the magnetic field measurements. The vertical magnetic field component may also be recorded. Processing of the recorded data with time variations of the electromagnetic field involves transformation into the frequency domain and calculation of the magnetotellurics impedance tensor Z and magnetic tipper function T=[A B] defined as follows:

$$\begin{bmatrix} E_x \\ E_y \end{bmatrix} = Z \cdot \begin{bmatrix} H_x \\ H_y \end{bmatrix} = \begin{bmatrix} Z_{xx} & Z_{xy} \\ Z_{yx} & Z_{yy} \end{bmatrix} \cdot \begin{bmatrix} H_x \\ H_y \end{bmatrix}$$

$$H_z = \begin{bmatrix} A & B \end{bmatrix} \cdot \begin{bmatrix} H_x \\ H_y \end{bmatrix}$$

where E_i is the electric field component in direction i and H_i is the magnetic field component in direction i. Subscripts i=x,y and z refer to a right angle coordinate system with z down. Information on dimensionality of the resistivity structures is provided by the tensor and tipper, which is used to guide the choice of principal models in inversion of the data. The tipper and diagonal elements of the impedance tensor are zero for 1D structures. In this case Z_{xy}=-Z_{yx}. Two dimensionality is indicated if the tensor has zero diagonal elements and $Z_{xy} \neq -Z_{yx}$ in a coordinate system with axis along and perpendicular to strike. The two directions are then referred as transverse electric (TE mode, all currents run along strike) and transverse magnetic (TM mode, currents perpendicular to strike).

The electromagnetic field decays exponentially with depth in a homogenous half space. A useful approximation with respect to depth of investigation is given by

$$d = 500[m]\sqrt{\frac{\rho[\Omega m]}{f[Hz]}}$$

where ρ is the resistivity and *f* is frequency. Thus, for a resistivity of 1 Ωm and frequency of 10^{-2} Hz, the depth of investigation is about 5 km.

The transformation of the measured time series into the impedance tensor and tipper function removes the information about the inducing primary field in the measured data and the tensor and tipper are solely dependent on the electrical structure of the earth. The source independency of the tensor and tipper is valid for the far-field approximation if artificial controlled sources are used as described in Li & Pedersen (1984) and Hughes & Carlson (1987). Disturbances from other artificial sources in the vicinity of the recordings site may exclude the possibility of obtaining data of sufficient quality.

The application of MT in hydrocarbon exploration is directed towards mapping of conductive alteration zones surrounding reservoirs. The increase in conductivity is mainly a result of disseminated pyrite. The presence of pyrite may also imply that induced polarization phenomena are associated with the presence of reservoirs.

3. Pedersen & Shan: Report on magnetotelluric measurements in the Tønder area, Denmark

Authors: Laust B. Pedersen and Chunling Shan
Uppsala University, Department of Earth Sciences,
Villavägen 16, 75653 Uppsala, Sweden

Date: October 22, 2012

INTRODUCTION

This report describes the results of a magnetotelluric (MT) survey carried out in the Tønder area, SW Denmark.

The area has a known occurrence of hydrocarbons as evidenced from several deep test wells, and it is covered by numerous 2D seismic lines and one 3D survey. The area shows similarities to areas in Germany and Poland with producing gas fields.

The area is also believed to be typical in the sense of electromagnetic noise conditions in Denmark, and it is interesting to find out as to whether standard MT measurements using natural sources are sufficiently robust to resolve the electrical resistivity structure down to basement levels.

We first give a short description of the processing of the recorded electromagnetic data including robust processing and 1D quality control of the major impedance elements. We then show the results of TE+TM inversion of the data along 7 NS directed profiles and finally a first attempt at constructing a 3D model using 3D inversion of all the data is presented.

Data and results are provided digitally on the enclosed DVD.

DATA ACQUISITION AND PROCESSING

Measurements took place from August 19 to August 31, 2012. Altogether 42 audiomagnetotelluric (AMT) sites were measured in the Tønder area in southern Denmark (Fig. 3.1). Data were collected within the period range approximately from 0.003s–100 s using the Uppsala-type magnetotelluric systems (MTU2000, Uppsala, Sweden).

The Uppsala pool of MT instruments consists of three broadband and eight long-period systems. The equipment utilizes 24-bit EarthData acquisition systems, which allow a maximum sampling rate of 3000 Hz and simultaneous sampling at two different frequencies (dual sampling mode). The electric field is measured using electrodes designed and built in Uppsala, similar to the Pb-PbCl type of Petiau (2000). Magnetic field components are measured with MetronixMFS06 (Braunschweig, Germany) induction coils for broad-band recordings. Broad-band data were recorded at each site in dual sampling burst mode for about half a day. Data at 1000 Hz were sampled for 2 hr (burst mode recording). Simultaneously, continuous data were acquired at 20 Hz sampling rate.

The GPS coordinates and recording times for the 42 stations are given in Table 1 together with remarks about special problems for certain stations. *Notice that for all stations the x-axis is directed along the magnetic north and the y-axis along the magnetic east, such that the z-axis is pointing vertically downwards.*

The broad-band measurements were performed with two instruments, the third instrument was operated simultaneously in northern Sweden close to Arvidsjaur, Sweden. It is anticipated that this remotely located station can be used to improve data quality in the frequency range 5-300 Hz. However, at the time of writing we have not yet received the data from this station. Besides the frequency band 5-300 Hz in the context of the Danish sedimentary basin is less important than the band 0.2-500 s, which for a 2 Ohm-m half-space corresponds to minimum and maximum depths of about 0.3 and 16 km, respectively. We tested the used of local remote references (Appendix A), but found no difference in quality of the estimated transfer functions, so throughout we have used the single station technique.

All the data were processed with a robust remote reference code (Smirnov 2003). The following transfer functions were estimated:
the magnetotelluric (MT) transfer function (impedance tensor **Z**), relating the horizontal electric field **E** and the horizontal magnetic field **H** as

$$\mathbf{E} = \mathbf{ZH};$$

or

$$\boldsymbol{E} = \begin{bmatrix} E_x \\ E_y \end{bmatrix} = \begin{bmatrix} Z_{xx} & Z_{xy} \\ Z_{yx} & Z_{yy} \end{bmatrix} \begin{bmatrix} H_x \\ H_y \end{bmatrix} = \mathbf{ZH}$$

and the geomagnetic depth sounding (GDS) transfer function (tipper vector **T**), relating the vertical magnetic field H_z to the horizontal magnetic field **H** as

$$H_z = [T_{xz} \quad T_{yz}] \begin{bmatrix} H_x \\ H_y \end{bmatrix} = \mathbf{TH}.$$

The processing parameters used for all stations are specified in Table 2. The most important parameters for the robust estimation scheme of Smirnov are the following.

- All segments are of length 32 samples.

- The first decimation level corresponds to the original sampling rate of 1000 Hz or 20 Hz. The whole time series is analyzed with these sampling rates and
- a coherence sorting is performed such that segments with predicted coherences less than 0.4 are automatically rejected.
- The harmonics 4-10 of the remaining segments are stored for the final robust estimation.
- The second decimation level corresponds to half the original sampling rate which is accomplished by low pass filtering of the total time series and resampling.
- The process is repeated with coherence sorting and storing of the new 4-10 harmonics of the remaining segments.
- This decimation is repeated up to ten times such that in each step the sampling rate is reduced by a factor of 2.
- In the final selection of segments only the 1000 best estimates in each frequency band is retained. In practice this means that for the higher frequencies only a small percentage of the total data is used for the estimation of the transfer functions, whereas for the lower frequencies most of the segments passing over the coherence sorting threshold are used for the final estimation of transfer functions.

It is customary to represent the off-diagonal elements of the impedance in the form of apparent resistivity (essentially the squared absolute value of the impedance) and the phase of the impedance. The processing software uses a time dependence of *exp(-iωt),*whereby Z_{xy} lies in the fourth quadrant of the complex plane and Z_{xy} in the second quadrant of the complex plane for most cases met in sedimentary basins.

QUALITY CONTROL

The Tønder area is generally very noisy with a lot of man-made disturbances on both electric and magnetic fields. The robust processing technique of Smirnov is capable of removing much of the bias introduced by such noise sources, even for a single station. Nevertheless it is a worthwhile exercise to make an analysis of quality of the transfer functions in order to identify stations with unreasonable transfer functions. The estimated impedance tensors and tipper vectors were examined separately.

For the impedance tensors we studied the off-diagonal elements using a 1D model representation by simply fitting them with the automatic 1D inversion method developed by Pedersen (2004). The results for all 42 stations are shown in detail in the folder **MTDK_2012\Results\1D_datafit_impedance.** Here only the results for station 6 are shown in Figure 3.2. The estimated impedance tensor (scaled by $\sqrt{\frac{T}{2\pi\mu_0}}$ in order to magnify the responses at longer periods, *T*) Notice that the model responses for the diagonal impedance elements are identically equal to zero. In this case the estimated diagonal impedance elements are also close to zero which is expected for a quasi-stratified sedimentary column. Large diagonal elements indicate noisy and possibly biased responses. A summary of the results for all stations is given in Table 3. The corresponding 1D models are shown in the folder **MTDK_2012\Results\1Dmodel_new**. In Figure 3.3 we show the 1D models along profile 4. We show the models to give a first impression of the stability and variation of the 1D models, but since no bonds have been used to bind the models together it must be understood that the models show quite some scatter, primarily due to scatter in the data, rather than representing a real variation in underground electrical resistivity from site to site. We will discuss the matter later in the section on modeling.

For the tipper vectors (vertical magnetic transfer functions) we only present the estimated values in the folder **MTDK_2012\Results\1D_datafit_impedance\Magnetic_TF.** It is interesting to note that for periods less than about 0.1 s the tipper vectors are heavily distorted, whereas the impedances are much more stable. This can be interpreted to indicate that the vertical magnetic field component is much more noise contaminated than the horizontal components in that period range. For that reason we will not make use of the tipper vectors for 2D modeling.

MODELLING

As mentioned before we have projected the stations onto six NS running profiles in order to allow for 2D modeling. The strike is largely EW and although the data do not indicate a clear geoelectrical strike because the impedance tensors appear to show 1D behavior, we assume that the more or less EW strike of the nearby Ringkøbing-Fyn high could have some effect on the structural trends in the Tønder area some 100 km to the south. Besides the length of the NS lines is longer than the corresponding EW lines and more stations are located on the NS lines.

The geoelectical structure in the study area is largely 1D. Nevertheless it is worthwhile model the data in 2D because the TE and TM modes must be satisfied by the same model, which adds further constraints onto the model than can be accomplished by fitting to individual XY and YX data with 1D models. Besides the inversion code by Kalscheuer et al. (2010) allows for emphasizing horizontal smoothness, expected to be dominant in sedimentary environments. Horizontal smoothness further has the effect of down-weighting the influence of bad, biased data, which are not expressed in their corresponding random data errors.

After cleaning the data by removing whole stations or parts of stations we ran individual TE and TM mode inversions as well as combined TE and TM inversions. In all cases to be shown we used error floors of 5% on TM apparent resistivity and 10% on TE apparent resistivity, whereas all phases had error floors of 5%, corresponding to approximately 3^{o}. The models and datafit for all 6 profiles with individual TE or TM inversions are shown in the folder **MTDK_2012\Results\2D_model+2D_datafit**, and the final models for joint TE+TM inversion are shown in the subfolder **TE+TM.png.zip**. A summary of the datafit for the 6 profiles and the different inversion runs are shown in table 4. Finally a number of slices through a 3D diagram of all 6 models is shown in Figure 3.5 as well as in the file **MTDK_2012\Results\2D_model_slices**.

A first attempt at 3D inversion of the full impedance tensor is presented in Figure 3.6 and in the folder **MTDK_2012\Results\3D_model_slices**. An error floor of 2.5% was imposed on the main impedance elements and the same error floor in absolute terms was imposed on the corresponding diagonal elements in the same row of the impedance tensor. Remember that for the 2D inversion we used an error floor of 5% on the apparent resistivity, which corresponds to the 2.5% error floor on the impedance. Since the station spacing is about 2.5 km it is necessary to regularize the inverse process to obtain smooth variations in the model between stations. Here we choose the horizontal smoothness to be five times greater than the vertical smoothness. The RMS data fit is 1.44 which is only slightly higher than the corresponding 2D RMS of about 1.0.

DISCUSSION AND CONCLUSIONS

The electromagnetic noise conditions in Denmark vary strongly on a local scale. It is thus important to have a dense network of MT sites in order be able to delete or down weight particularly noise contaminated sites from the 2D and 3D inversion stages. 1D inversion of the main impedance elements is a useful way of identifying such noisy stations in a sedimentary environment where extreme lateral variations in electrical resistivity as typically found in crystalline terrains are not expected.

The 2D inverse models generally support the conclusions derived from the 1D models, namely that there are three domains, an upper resistive domain of 400 m thickness underlain by a very conductive domain extending down to about 3000 m followed by a more resistive domain with gradually increasing resistivity. However, the models also show significant lateral variations along the profiles as well as variations across the profiles.

The 3D inverse models generally show more structure than the 2D models in the sense that conductors become more conductive and resistors more resistive. At this stage no analysis of the stability of the 3D models has been carried out and no comparison with the seismic results have been undertaken since this is beyond the scope of this report. Such a comparison is necessary to finally judge as to whether the results obtained are useful for getting an improved understanding of the variability of the lithological units in the area.

FIGURES

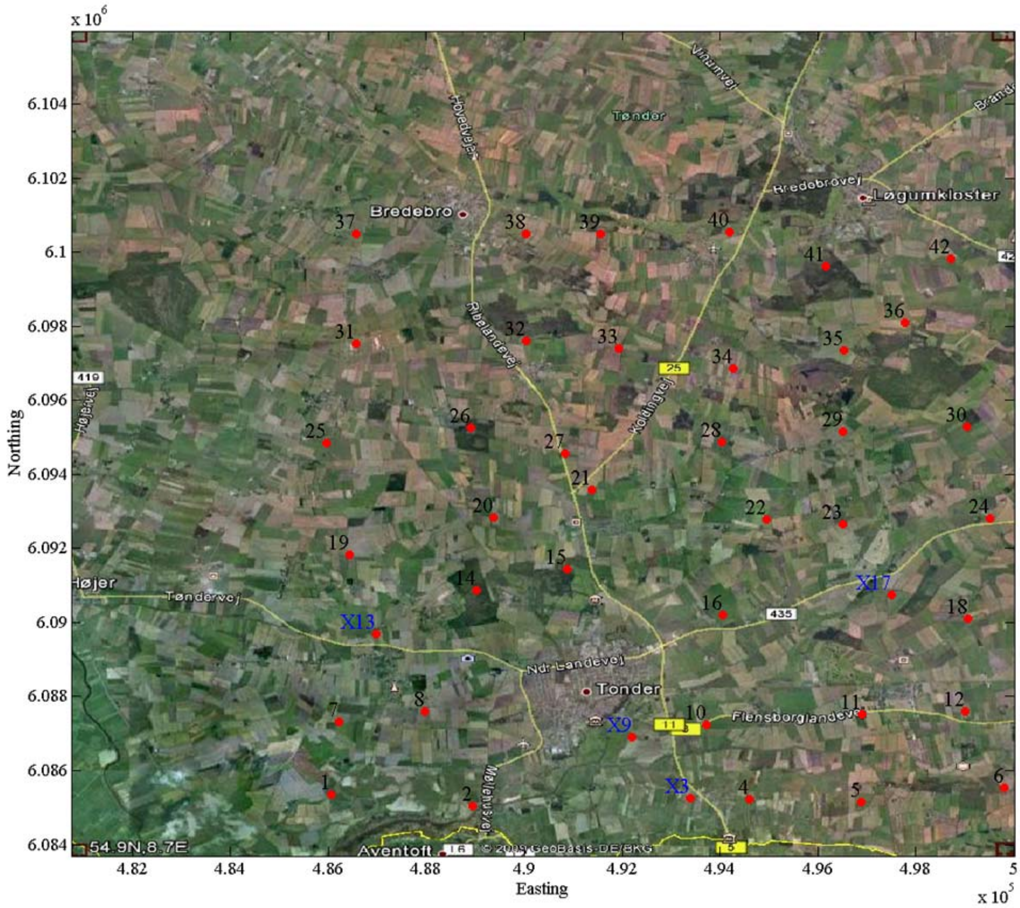

Figure 3.1a. Location of MT stations. Particularly noisy stations are indicated in blue.

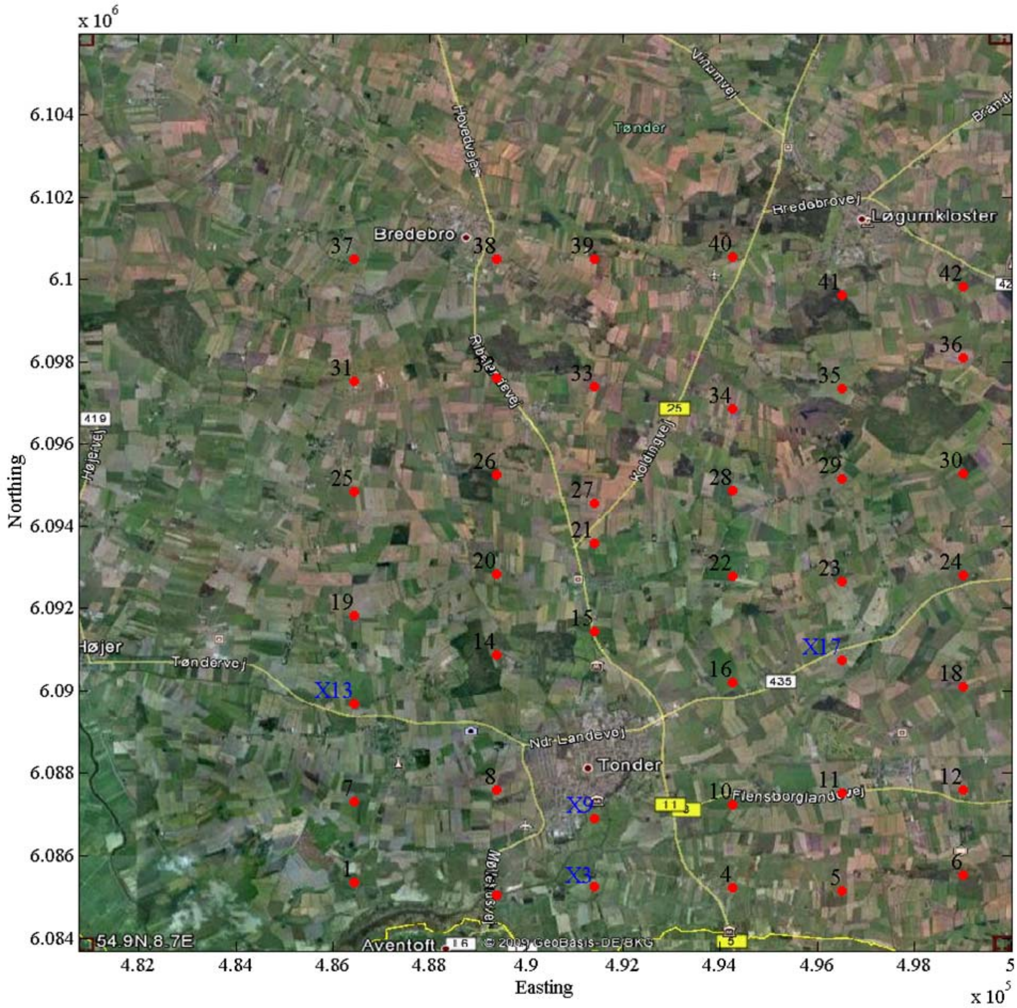

Figure 3.1b. Projected locations of MT stations. Projection onto NS lines imitating measurement profiles for 2D modeling. Lines are numbered 1 to 6 going from West towards East.

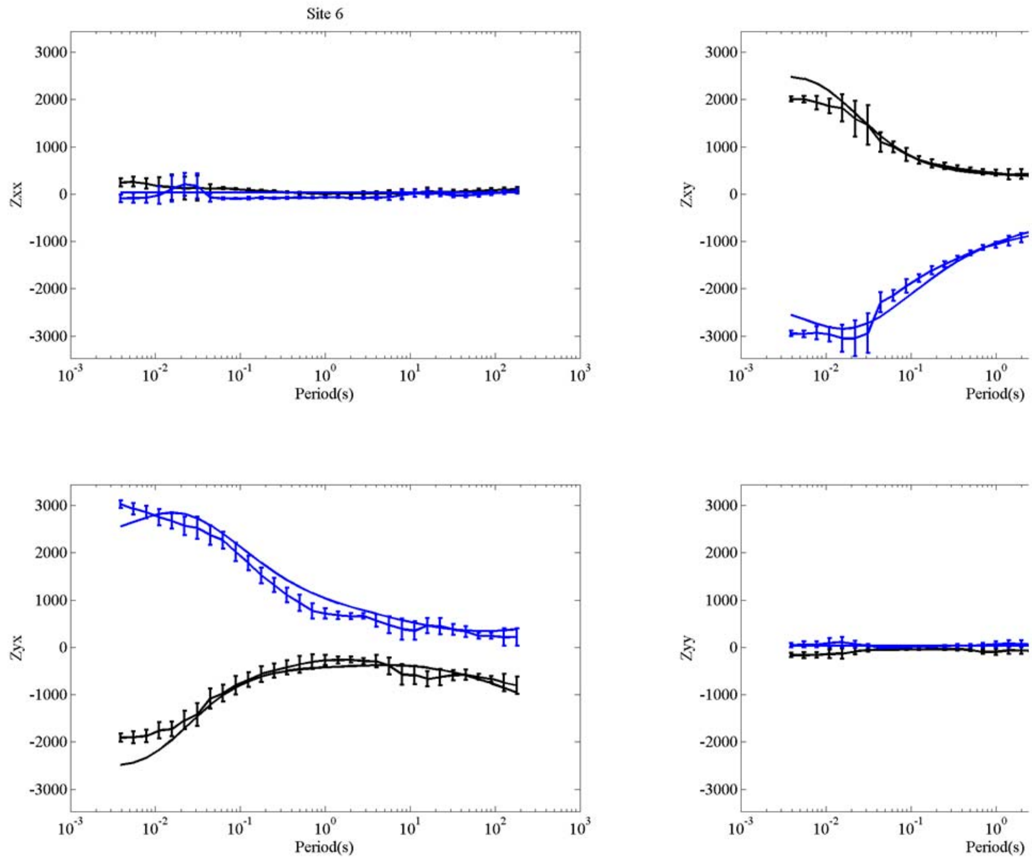

Figure 3.2. The estimated impedance tensor (scaled by $\sqrt{\frac{T}{2\pi\mu_0}}$) and the corresponding 1D model responses for station 6. Real part: black color with error bars. Imaginary part: blue color with error bars. 1D model responses are shown as black and blue lines without error bars for the real and imaginary parts, respectively. Notice that the model responses for the diagonal impedance elements are identically equal to zero. In this case the estimated diagonal impedance elements are also close to zero.

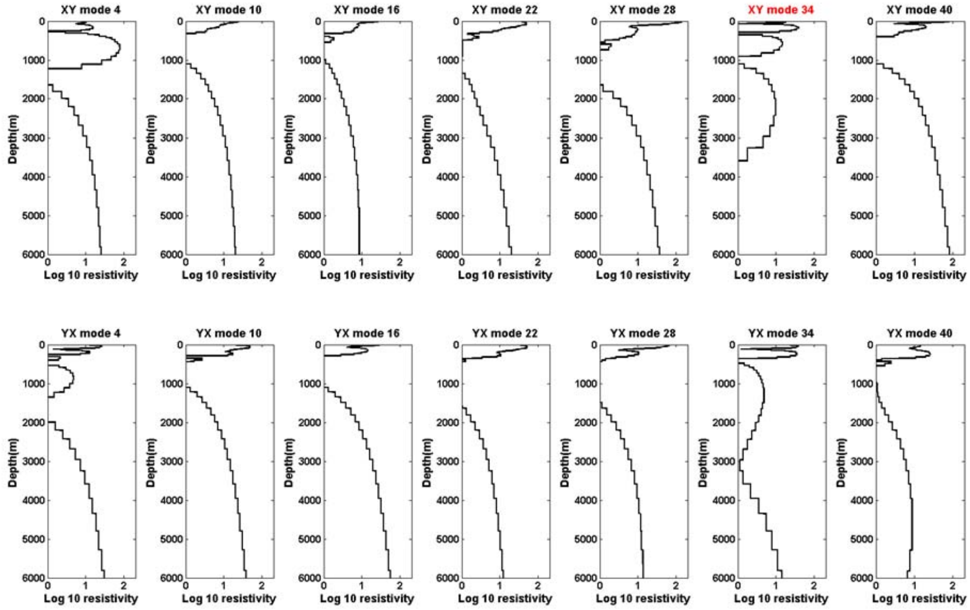

Figure 3.3. 1D models along profile 4. Upper row corresponds to current flow along the profile (NS). Lower row corresponds to current flow across the profile (EW). Red label indicates a particularly bad station (mode). Models largely indicate a three domains, an upper resistive domain of about 400 m thickness underlain by a very conductive domain extending down to ca 2000 m followed by a more resistive domain gradually increasing resistivity.

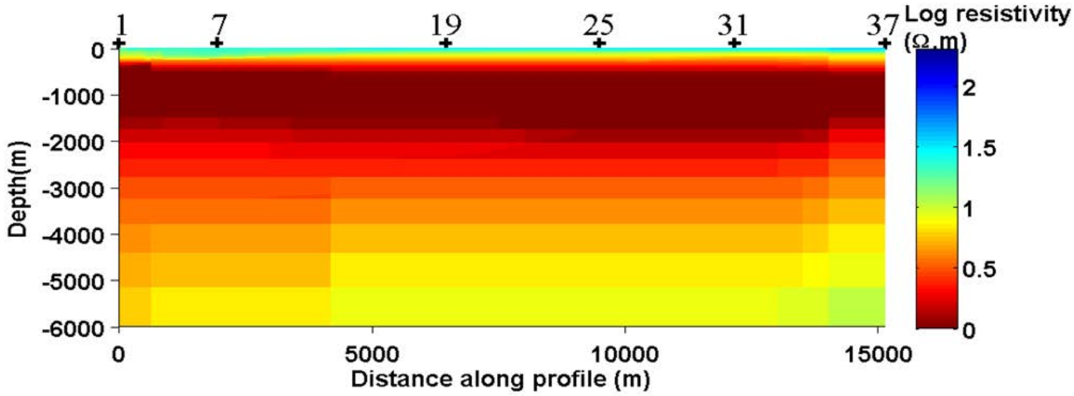

Figure 3.4a Joint inversion of TE+TM data along profile 1.

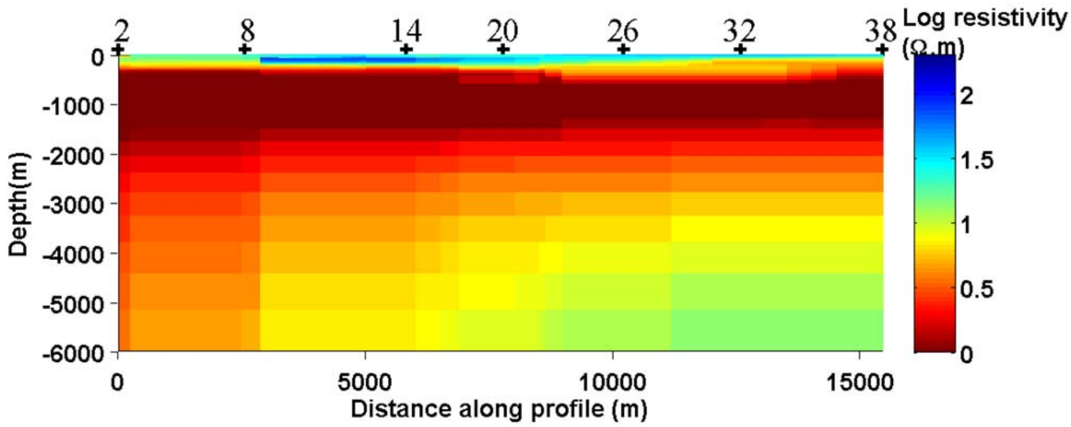

Figure 3.4b Joint inversion of TE+TM data along profile 2.

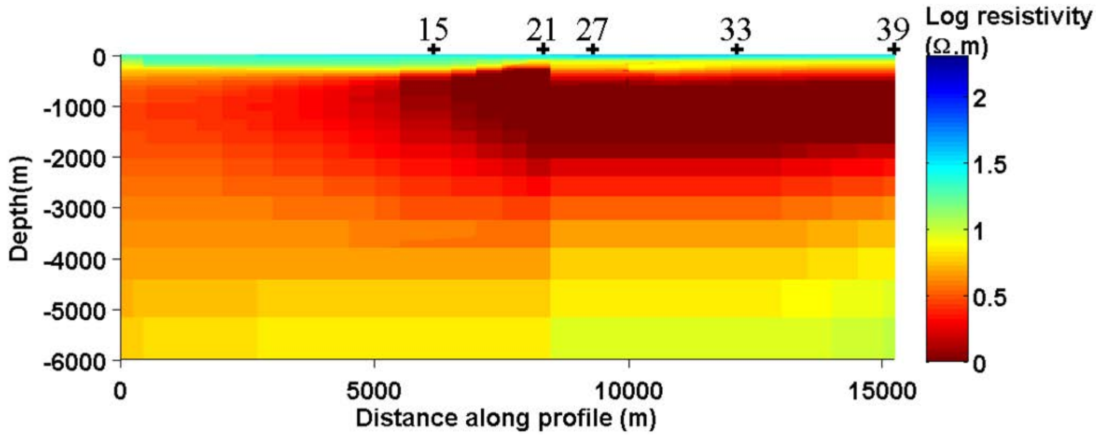

Figure 3.4c. Joint inversion of TE+TM data along profile 3.

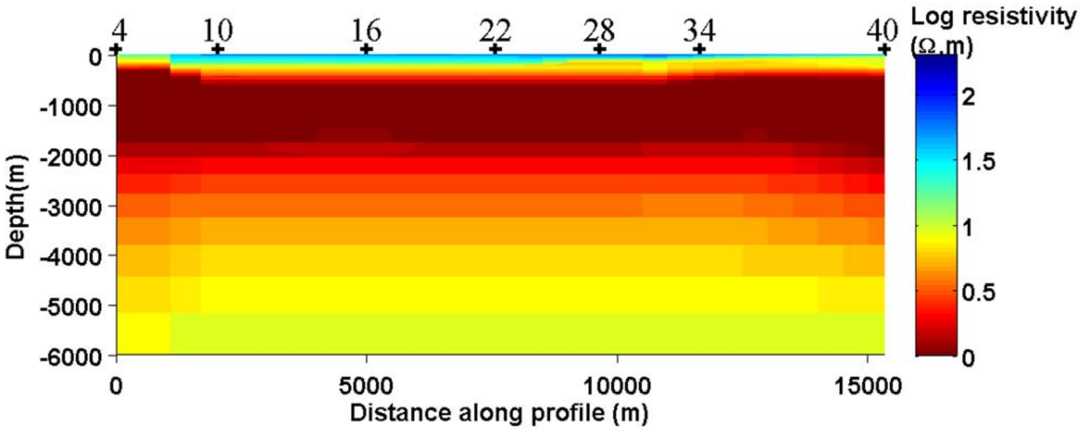

Figure 3.4d. Joint inversion of TE+TM data along profile 4.

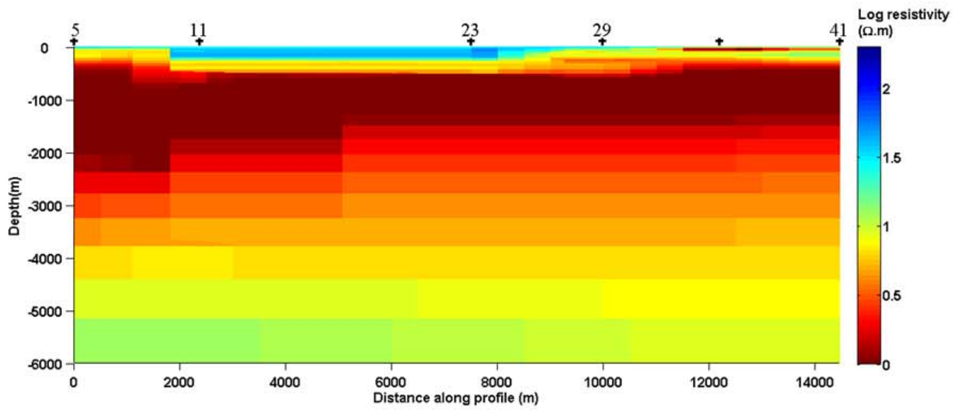

Figure 3.4e. Joint inversion of TE+TM data along profile 5.

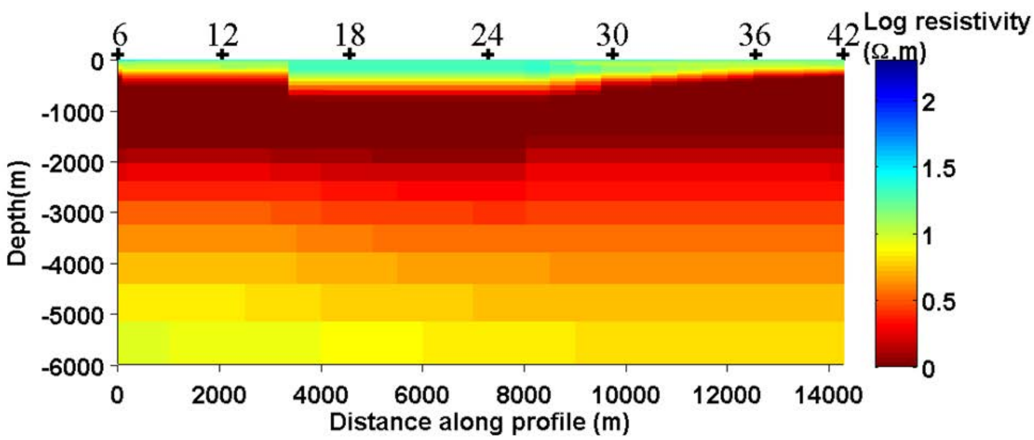

Figure 3.4f. Joint inversion of TE+TM data along profile 6.

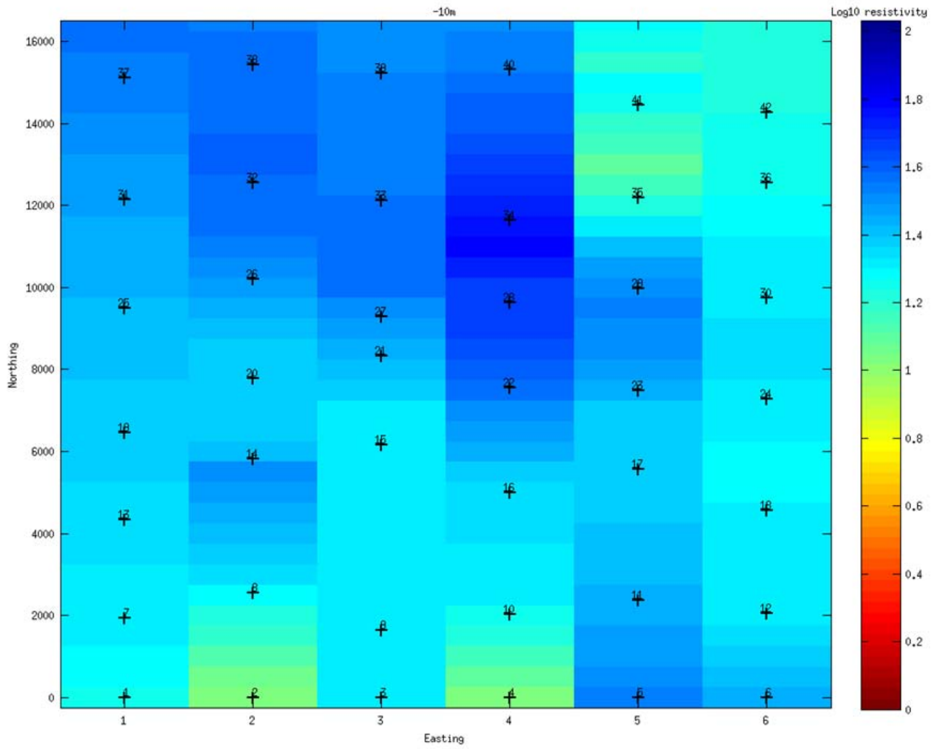

Figure 3.5a: 3D view of the 2D models of electrical resistivity along each of the 6 profiles numbered from W to E and distance along profile counted from S to N. Depth slice at 10 m.

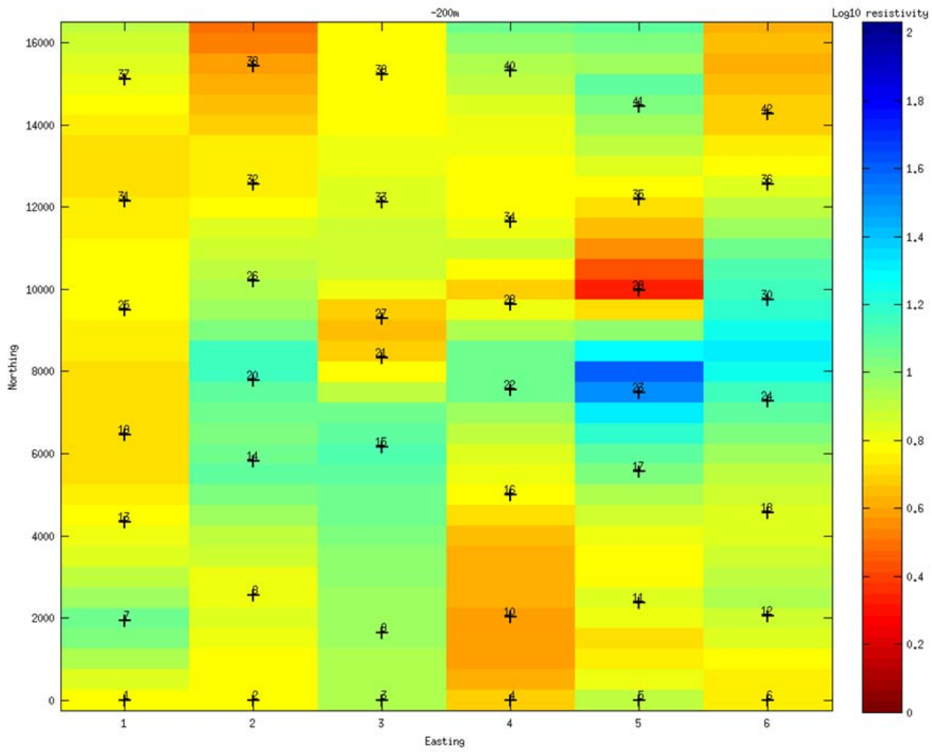

Figure 3.5b: 3D view of the 2D models of electrical resistivity along each of the 6 profiles numbered from W to E and distance along profile counted from S to N. Depth slice at 200 m.

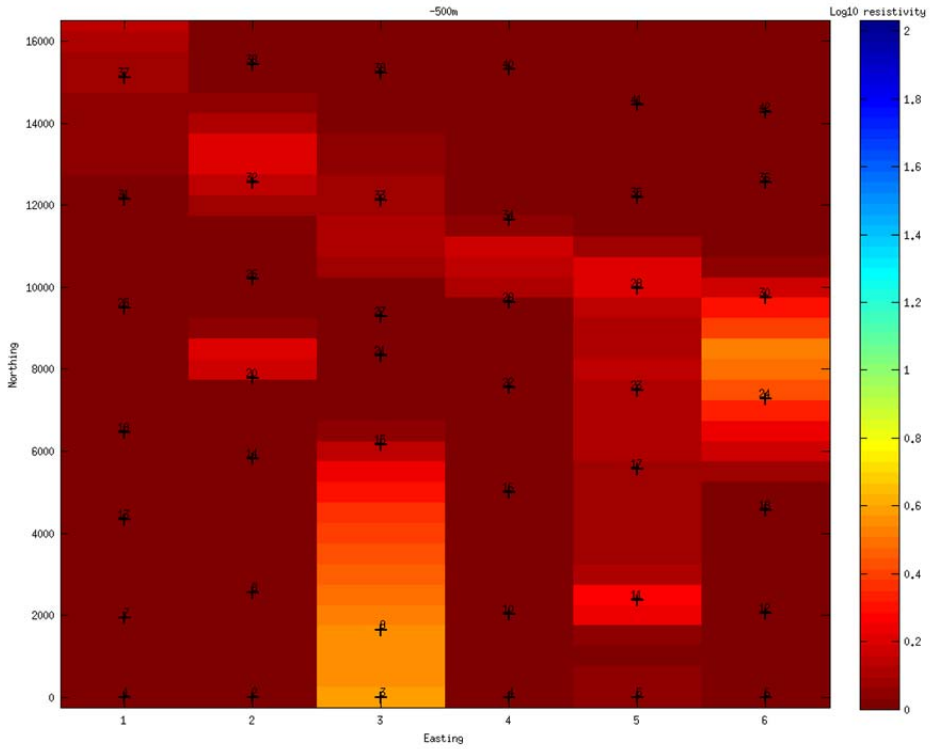

Figure 3.5c: 3D view of the 2D models of electrical resistivity along each of the 6 profiles numbered from W to E and distance along profile counted from S to N. Depth slice at 500 m..

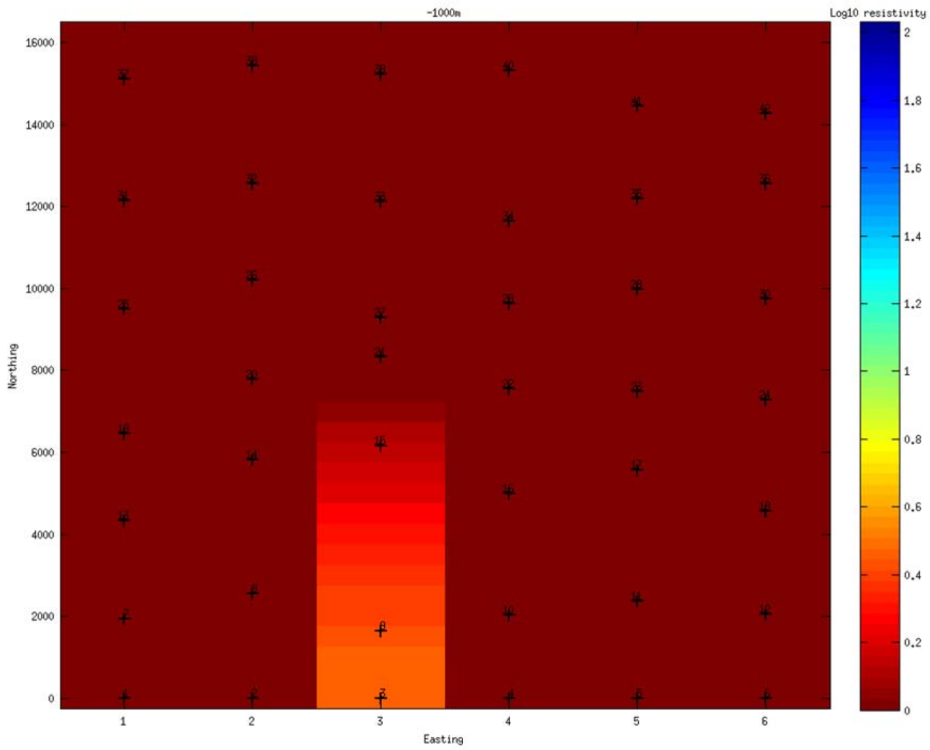

Figure 3.5d: 3D view of the 2D models of electrical resistivity along each of the 6 profiles numbered from W to E and distance along profile counted from S to N. Depth slice at 1000 m

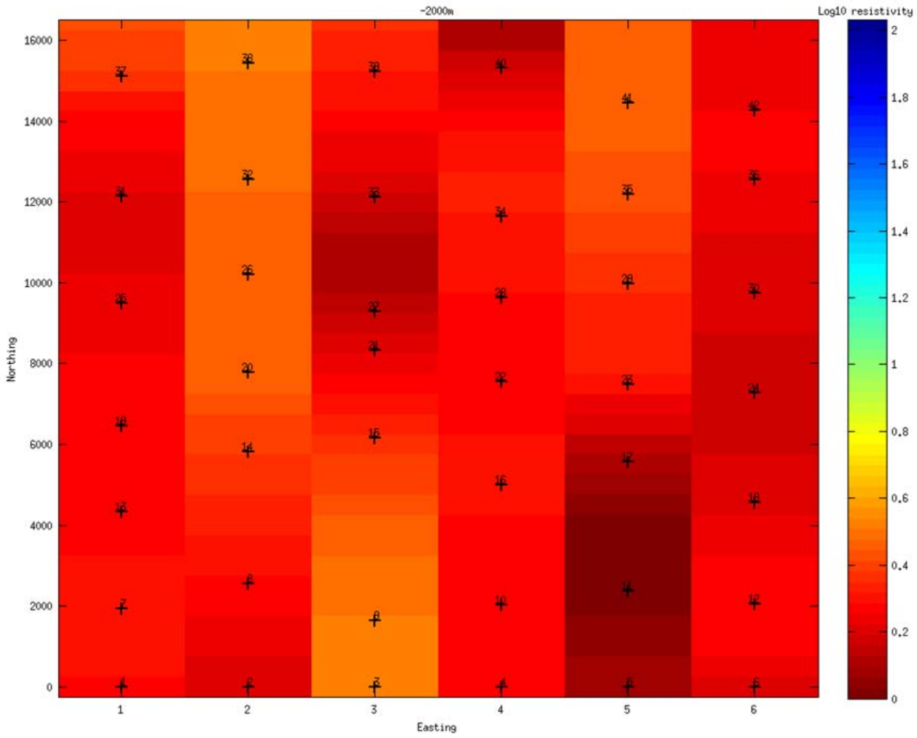

Figure 3.5e: 3D view of the 2D models of electrical resistivity along each of the 6 profiles numbered from W to E and distance along profile counted from S to N. Depth slice at 2000 m

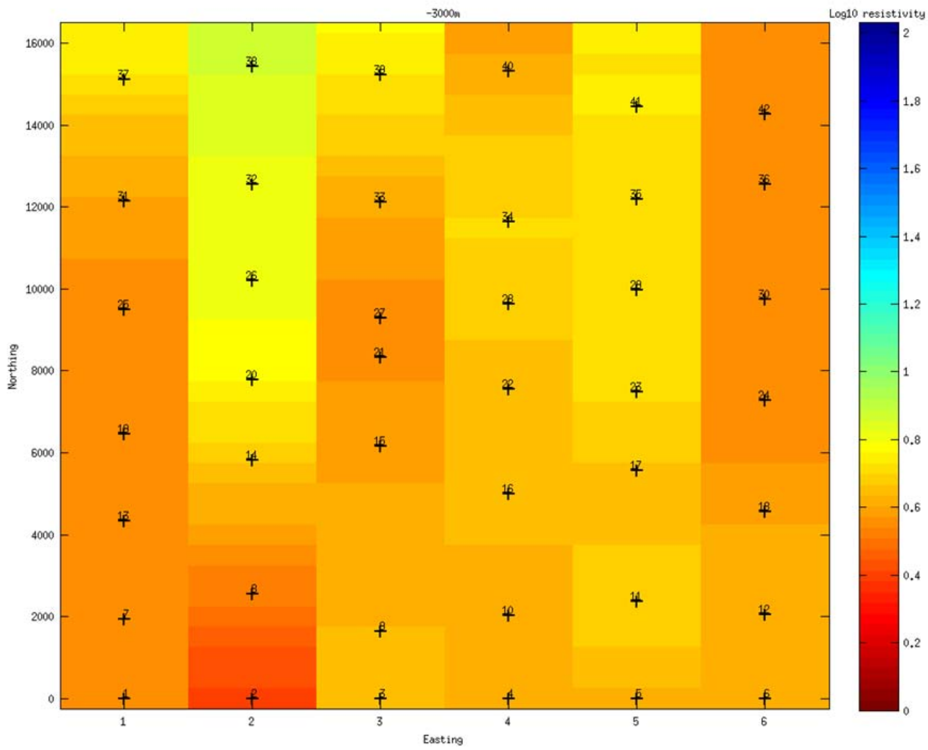

Figure 3.5f: 3D view of the 2D models of electrical resistivity along each of the 6 profiles numbered from W to E and distance along profile counted from S to N. Depth slice at 3000 m

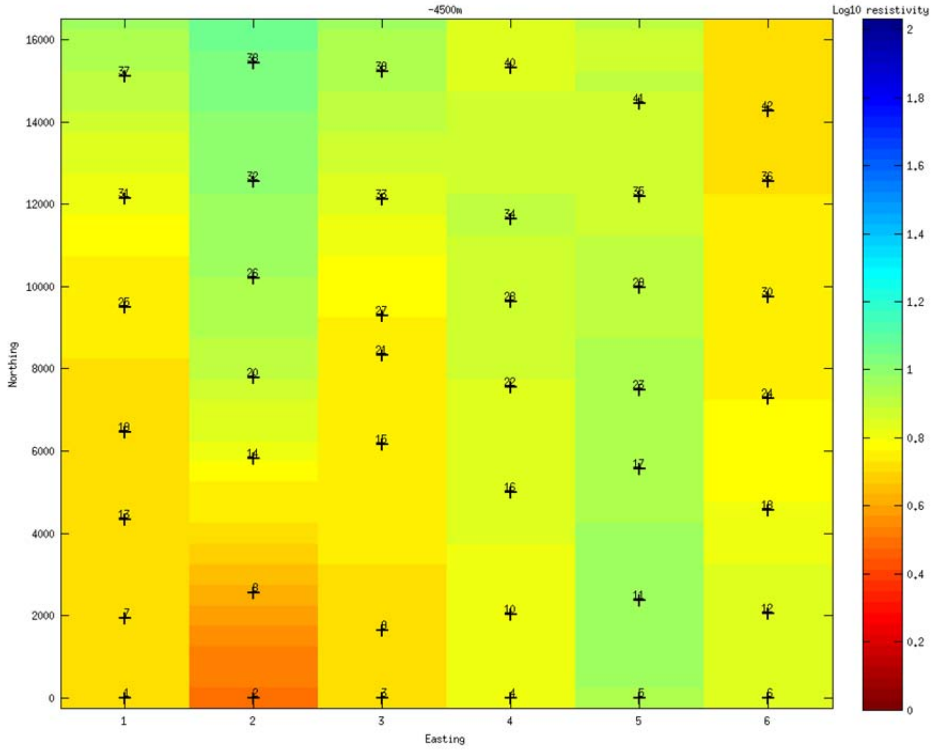

Figure 3.5g: 3D view of the 2D models of electrical resistivity along each of the 6 profiles numbered from W to E and distance along profile counted from S to N. Depth slice at 4500 m

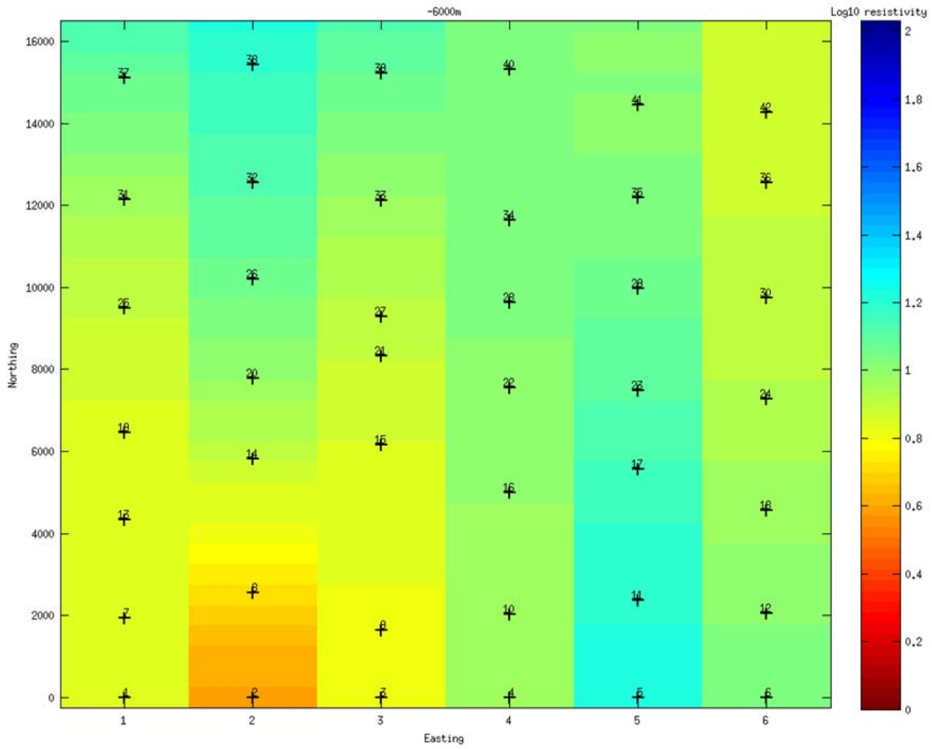

Figure 3.h. 3D view of the 2D models of electrical resistivity along each of the 6 profiles numbered from W to E and distance along profile counted from S to N. Depth slice at 6000 m

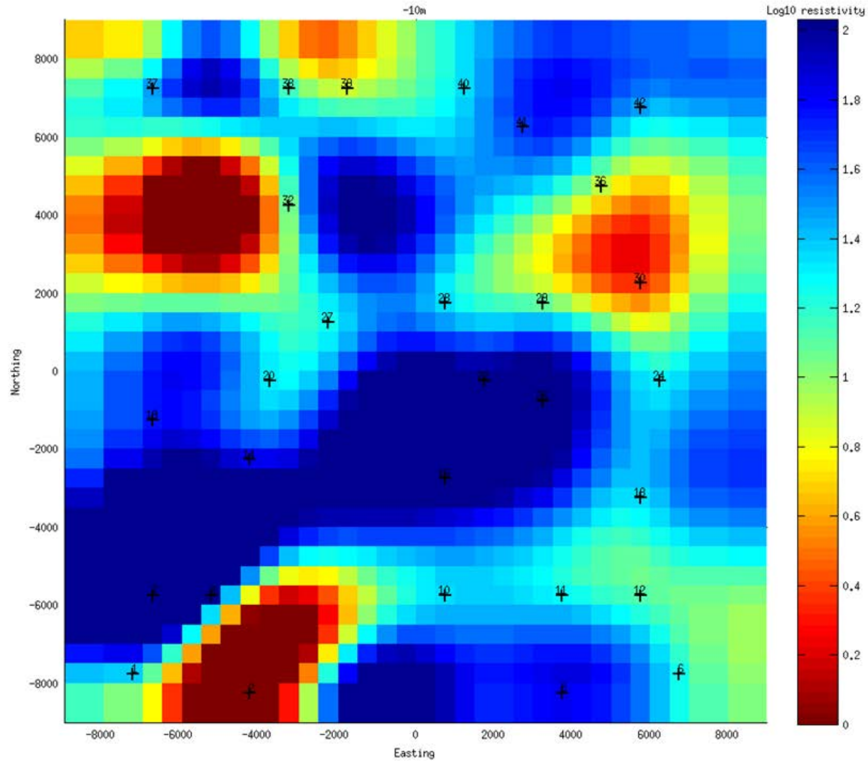

.

Figure 3.6a. 3D model based upon inversion of the full impedance tensor. Iteration number 4, RMS=1.44. Depth slices from top to bottom: Depth slices at 10 m

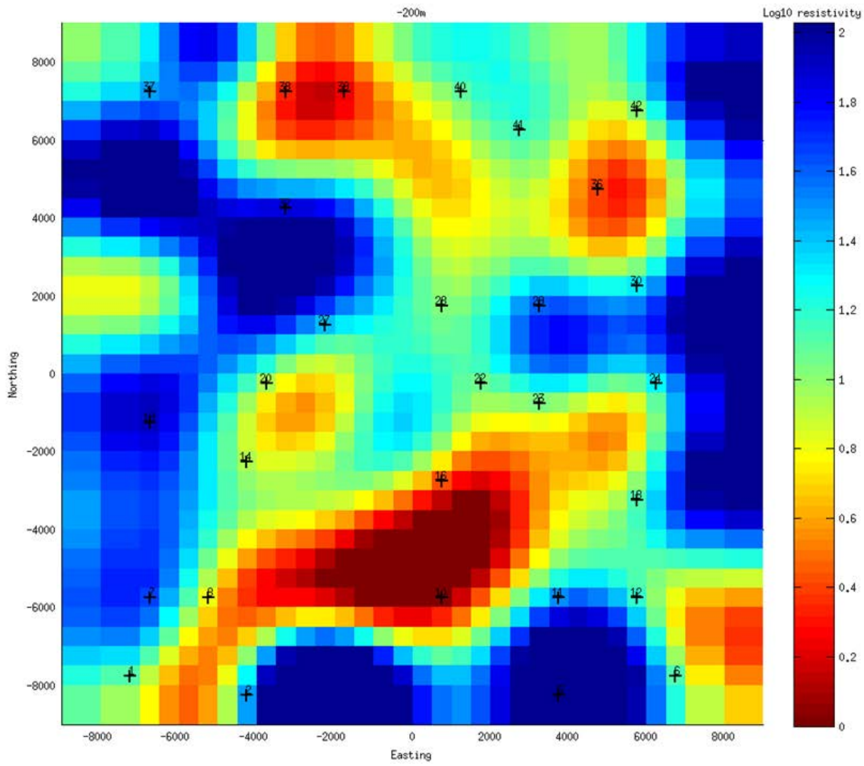

Figure 3.6b. 3D model based upon inversion of the full impedance tensor. Iteration number 4, RMS=1.44. Depth slices from top to bottom: Depth slices at 200 m

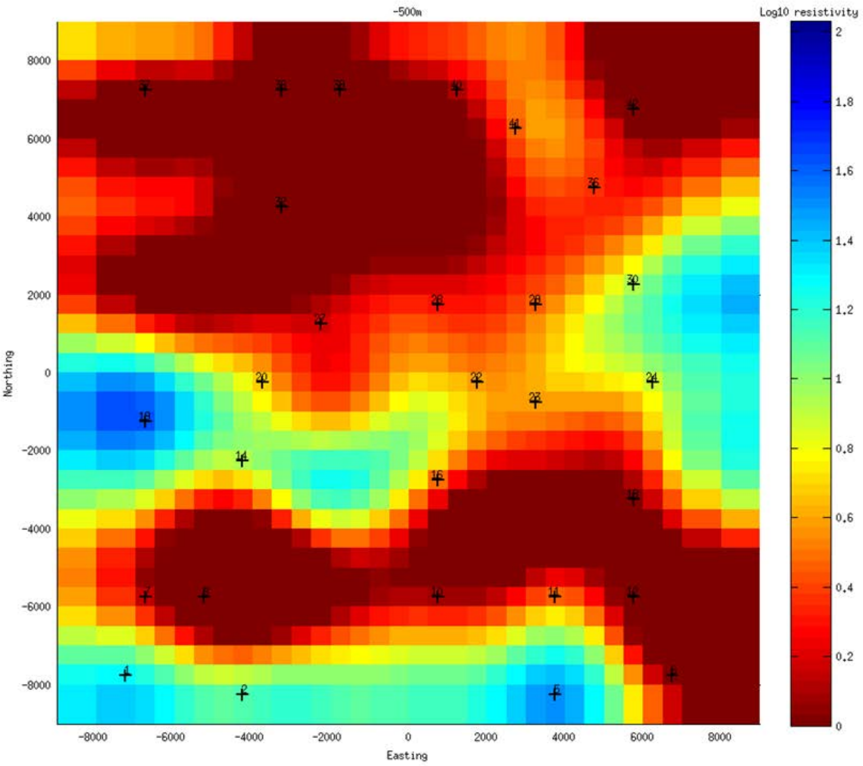

Figure 3.6c. 3D model based upon inversion of the full impedance tensor. Iteration number 4, RMS=1.44. Depth slices from top to bottom: Depth slices at 500 m

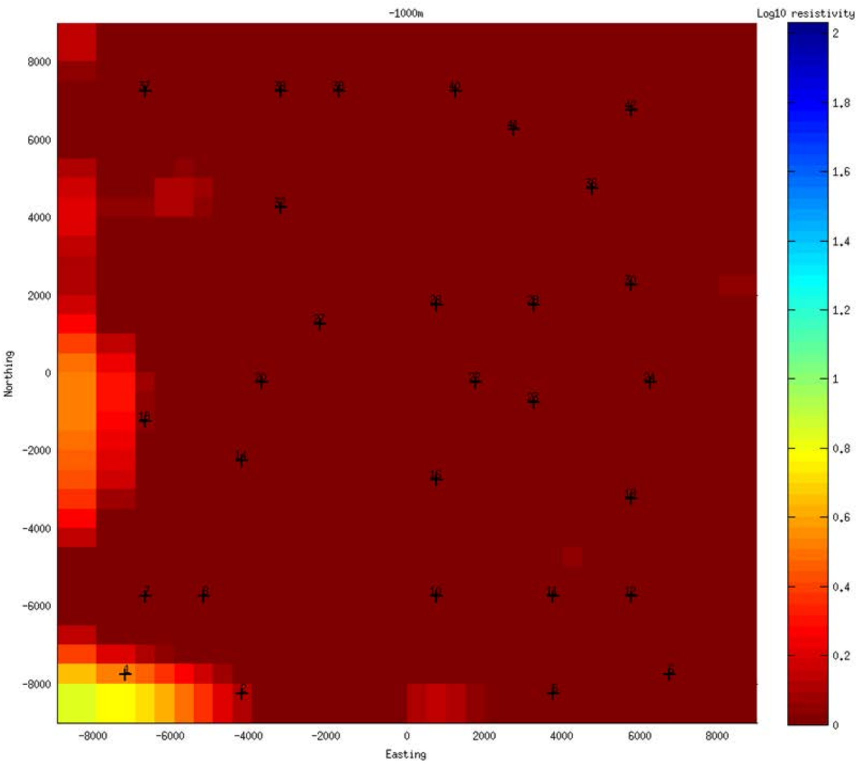

Figure 3.6d. 3D model based upon inversion of the full impedance tensor. Iteration number 4, RMS=1.44. Depth slices from top to bottom: Depth slices at 1000 m

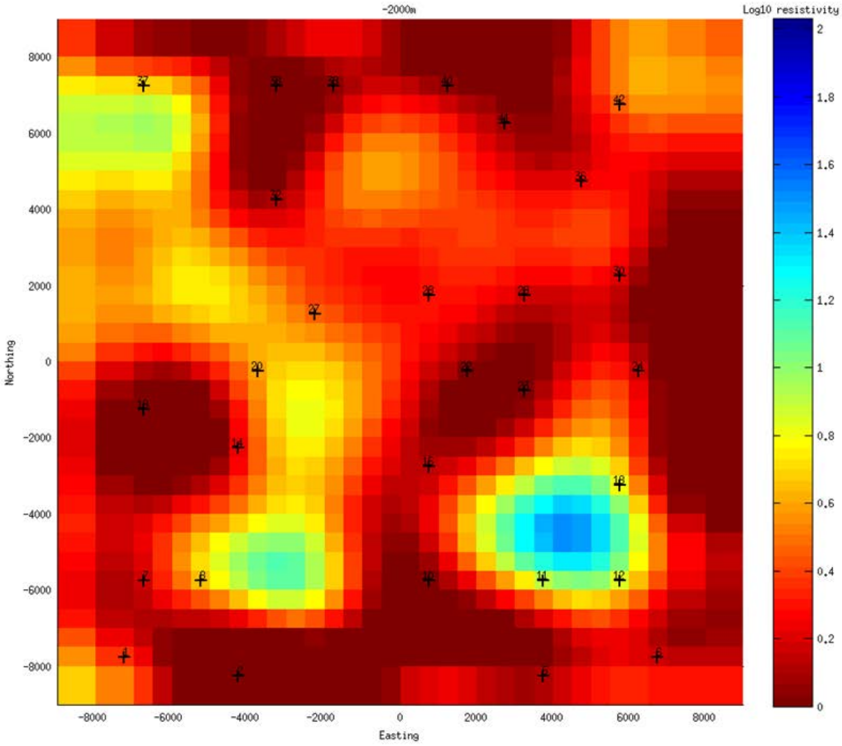

Figure 3.6e. 3D model based upon inversion of the full impedance tensor. Iteration number 4, RMS=1.44. Depth slices from top to bottom: Depth slices at 2000 m

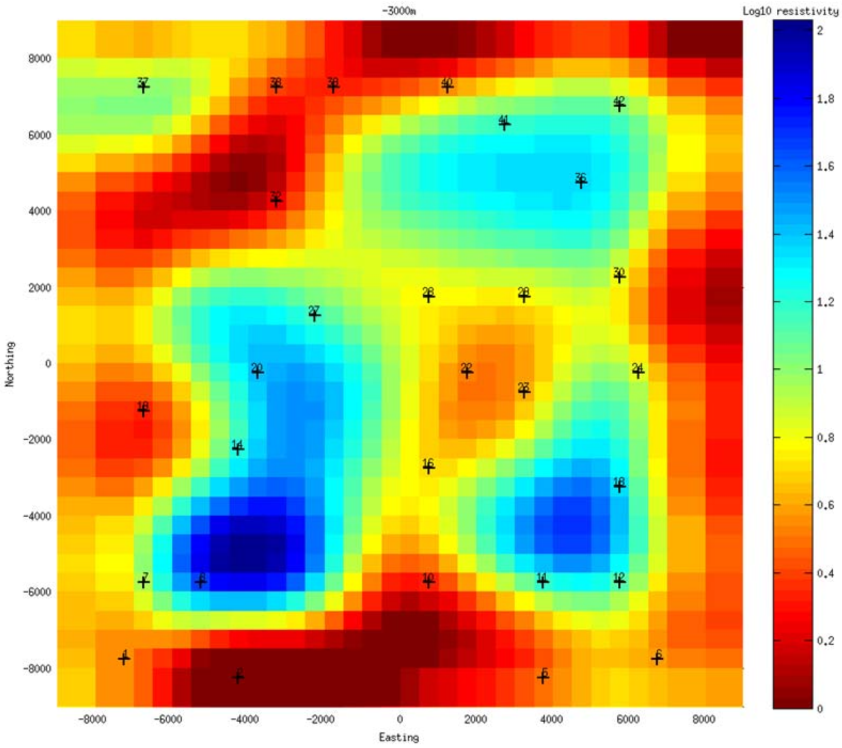

Figure 3.6f. 3D model based upon inversion of the full impedance tensor. Iteration number 4, RMS=1.44. Depth slices from top to bottom: Depth slices at 3000 m

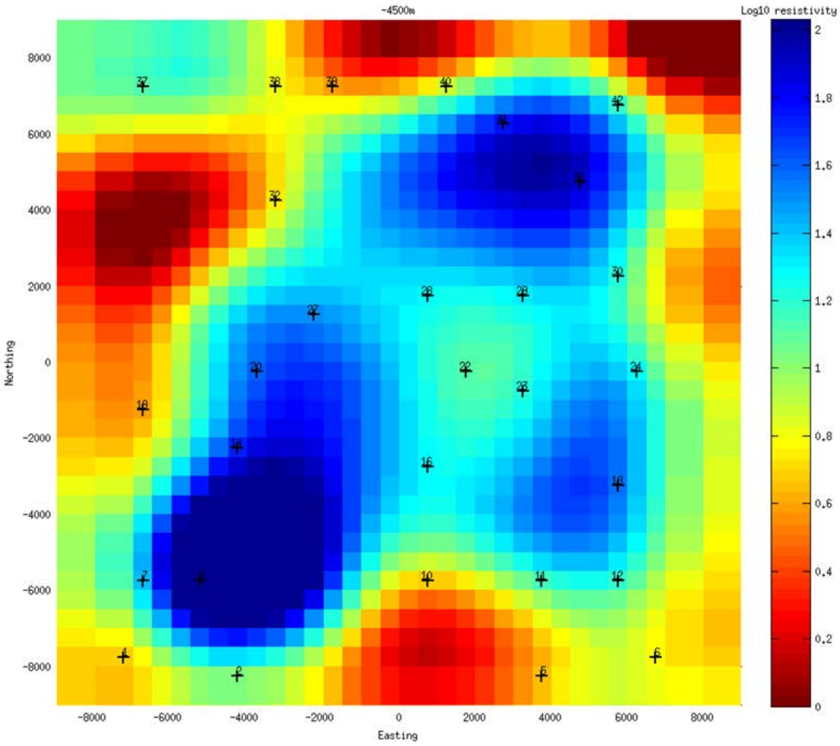

Figure 3.6g. 3D model based upon inversion of the full impedance tensor. Iteration number 4, RMS=1.44. Depth slices from top to bottom: Depth slices at 4500 m

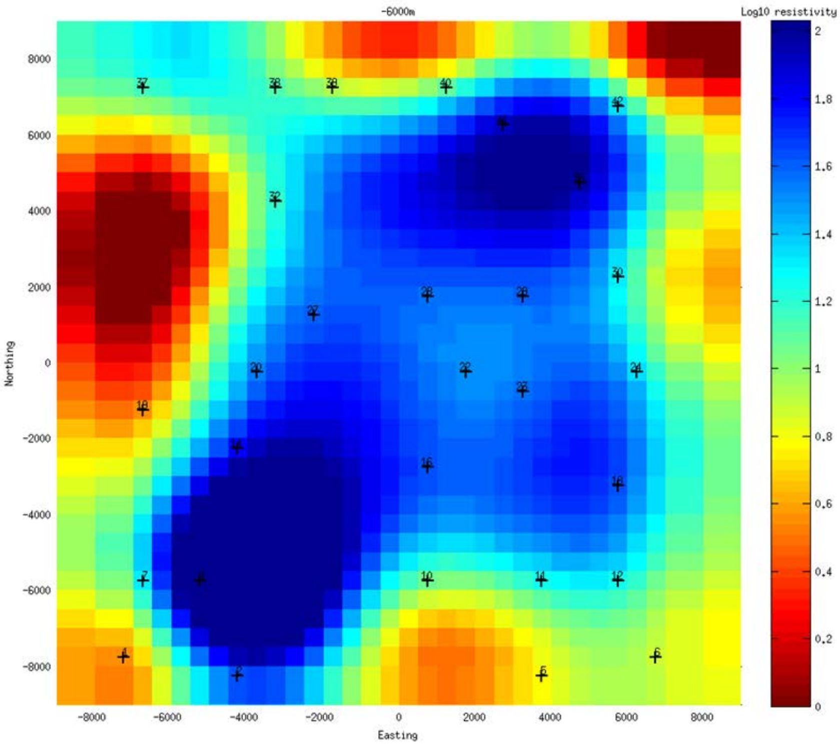

Figure 3.6h. 3D model based upon inversion of the full impedance tensor. Iteration number 4, RMS=1.44. Depth slices from top to bottom: Depth slices at 4500 m

TABLES

Table 1. Recording information for MT stations, August 19-31, 2012. See file **MTDK_2012\Results\Table\Recording_information**

STATISTICS	SIEGEL	Siegel robust statistics
STAT EVENTS	1000	Limits the number of segments used in Siegel statistics
FFT	32	Segment length for FFT
FFT_LI	4	Lowest harmonic used for estimation
FFT_HI	10	Highest harmonic used for estimation
NOTCHES	1	50 Hz and harmonics notched out
FMEDIAN	1	Spectral median filter to suppress outliers not removed by the nothes
COH_X	0.4	Coherence threshold for Ex
COH_Y	0.4	Coherence threshold for Ey
COH_Z	0.4	Coherence threshold for Hz
DECIMATIONS	10	Number of decimation steps
	7	Number of estimates per decade

Table 2. Processing parameters used in the Smirnov processing program.

Station number	$\lvert T_{zx} \rvert, \lvert T_{zy} \rvert$ (T is period in seconds)	Z_{xy}	Z_{yx}
1	T > 0.2s ok	ok	ok
2	/	ok	ok
3	/	/	/
4	ok	ok	ok
5	/	ok	ok
6	ok	ok	ok
7	T > 0.1s ok	ok	ok
8	T > 0.1s ok	ok	ok
9	ok	/	/
10	ok	ok	ok
11	ok	ok	ok
12	ok	ok	ok
13	/	/	/
14	T > 0.1s ok	ok	ok
15	ok	ok	ok
16	ok	ok	ok
17	ok	/	/
18	T > 0.3s ok	ok	ok
19	/	ok	ok
20	ok	ok	ok
21	ok	ok	ok
22	ok	ok	ok
23	T > 0.1s ok	ok	ok
24	T > 0.1s ok	ok	ok
25	T > 1s ok	T > 0.1s ok	T > 0.1s ok
26	ok	/	ok
27	ok	ok	ok
28	ok	ok	ok
29	ok	ok	ok
30	ok	ok	ok
31	ok	/	Ok
32	/	ok	ok
33	T > 1s ok	ok	Ok
34	/	ok	ok
35	T > 0.1s ok	ok	ok
36	/	ok	ok
37	T > 0.1s ok	ok	ok
38	T > 0.1s ok	/	ok
39	T > 0.1s ok	ok	ok
40	T > 0.1s ok	ok	ok
41	T > 0.1s ok	ok	ok
42	T > 0.1s ok	ok	ok

Table 3. Summary of quality check for tipper elements T_{zx} , T_{zy} and impedance elements Z_{xy} , Z_{yx}, respectively. Notice that tipper elements for periods less than 0.1 s are often seriously distorted, while impedance elements are still usable.

Profile Number	Site used for TM mode inversion	Site used for TE mode inversion	Final RMS TE	Final RMS TM	Final RMS TE+TM	Given error floor on resistivity TE	Given error floor on phase TE	Given error floor on resistivity TM	Given error floor on phase TM
1	1,7,19,37	1,7,19,25,31,37	0.99	0.98	0.98	10%	5%	5%	5%
2	2,8,14,20,32,38	2,8,14,20,26,32,38	1.00	1.01	0.99	10%	5%	5%	5%
3	27,39	15,21,27,39	0.98	0.97	0.98	10%	5%	5%	5%
4	10,16,22,28,40	4,10,16,22,28,34,40	0.95	0.98	0.99	10%	5%	5%	5%
5	5,11,23,29,41	5,11,23,29,41	0.98	1.28	1.28	10%	5%	5%	5%
6	6,12,18,24,30,36,42	6,12,18,24,30,36,42	0.98	0.98	0.99	10%	5%	5%	5%

Table 4. Summary of station distribution and RMS datafit for individual TE and TM as well joint TE+TM inversions. For the inversion of each profile, the horizontal smoothness is weighted four times higher than the vertical smoothness.

REFERENCES – Uppsala Report

Kalscheuer, T., Juanatey, M. d. l. A. G., Meqbel, N., Pedersen, L. B., 2010. Non-linear model error and resolution properties from two-dimensional single and joint inversions of direct current resistivity and radiomagnetotelluric data. Geophysical Journal International 182 (3), 1174–1188.

Pedersen, L.B., 2004. Determination of the regularization level of truncated singular-value decomposition inversion: The case of 1D inversion of MT data , Geophysical Prospecting 52, 261-270. Doi: 10.1111/j.1365-2478.2004.00414.x.

Petiau, G., 2000. Second generation of lead-lead chloride electrodes for geophysical applications, Pure Appl. Geophys., 157(3), 357–382.

Smirnov, M.Y, 2003. Magnetotelluric data processing with a robust statistical procedure having a high breakdown point. Geophysical Journal International, 152, 1-7.

APPENDIX A – Uppsala Report: Comparing single station and local remote reference estimates of transfer functions.

The idea behind using the horizontal magnetic field from a reference station in addition to the horizontal local magnetic field for estimation of transfer functions is to reduce the bias effects introduced by noise on the input (i.e. the horizontal magnetic channels) of the Earth's linear system with the electric channels and the vertical magnetic channels as output. However, as we shall see the bias effect apparently is not a big problem when using the processing approach of Smirnov

We present a few examples of remote reference processing using local references and compare with the corresponding single station processing results. All figures with the results of both impedance and tipper vector can be found in the folder **MTDK_2012\Results\Reference_example.** Here we only refer to the impedance estimates because only they are useful for interpretation in this case.

The first example is from station 22 using station 23 as a reference. Apparent resistivities and phases are shown in Figure A1.1 and A1.2, respectively. In this example data quality is good and there is very little difference between the estimates.

The second example is from station 25 using station 26 as a reference. Apparent resistivities and phases are shown in Figure A2.1 and A2.2, respectively. In this example data quality is less good and there is a bigger scatter between estimates than in the first example. The single station estimates seem to be less scattered than the reference station data as expected when the reference station is also noisy. But there is no evidence that bias effects are present in the single station estimates.

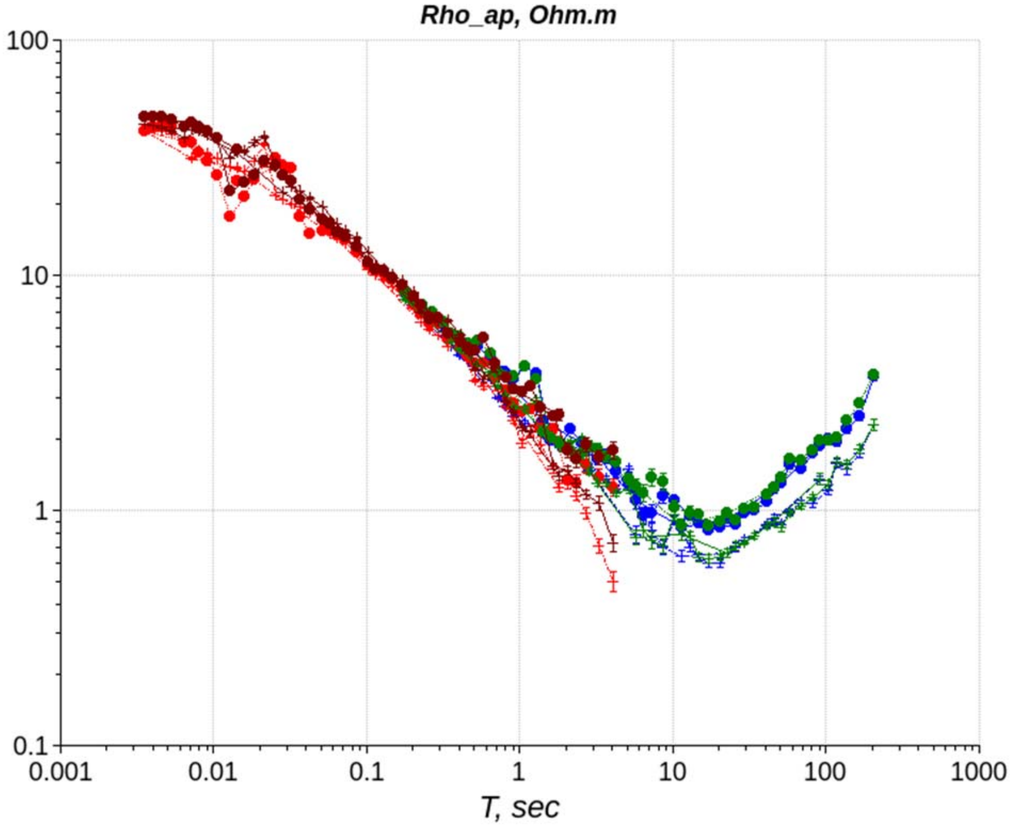

Figure A1.1. Comparison between single station and local remote reference estimation of apparent resistivities in x- and y-directions for station 22 using station 23 as a reference. Circles denote xy and crosses denote yx components of the apparent resistivity.
20 Hz sampling rate: Blue=single station; Green=reference station.
1000 Hz sampling rate: Light red=single station; Dark red=reference station.

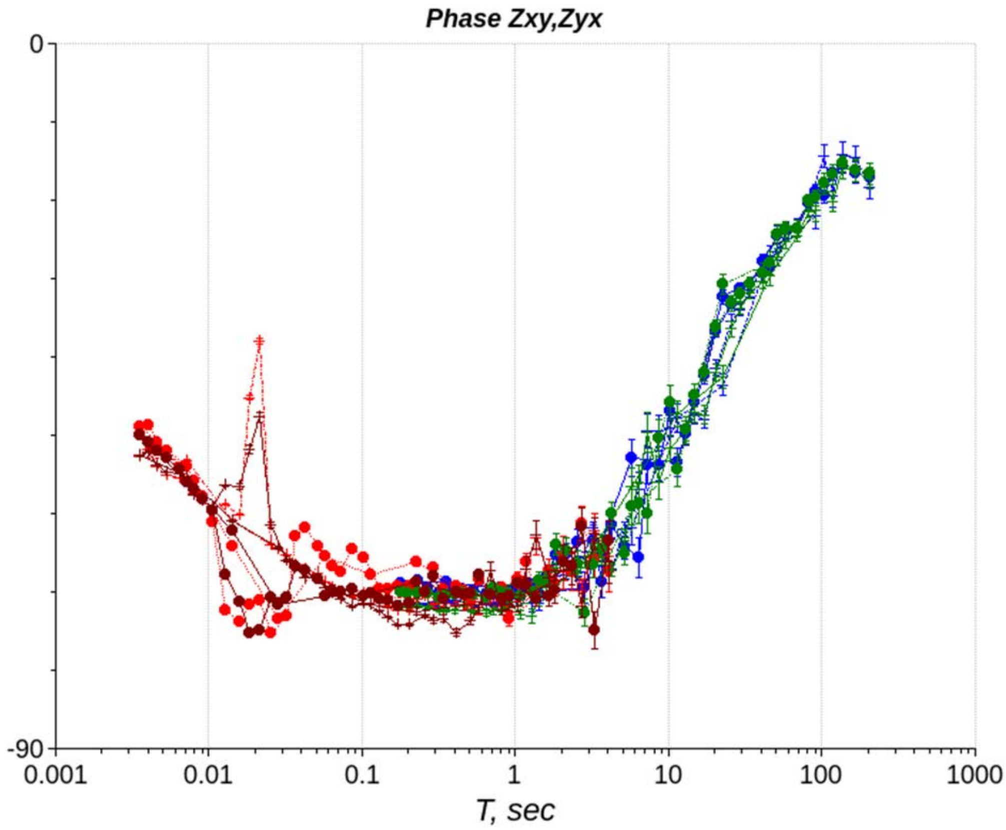

Figure A1.2. Figure A1.1. Comparison between single station and local remote reference estimation of phases in x- and y-directions for station 22 using station 23 as a reference. Circles denote xy and crosses denote yx components of the apparent resistivity.
20 Hz sampling rate: Blue=single station; Green=reference station.
1000 Hz sampling rate: Light red=single station; Dark red=reference station.

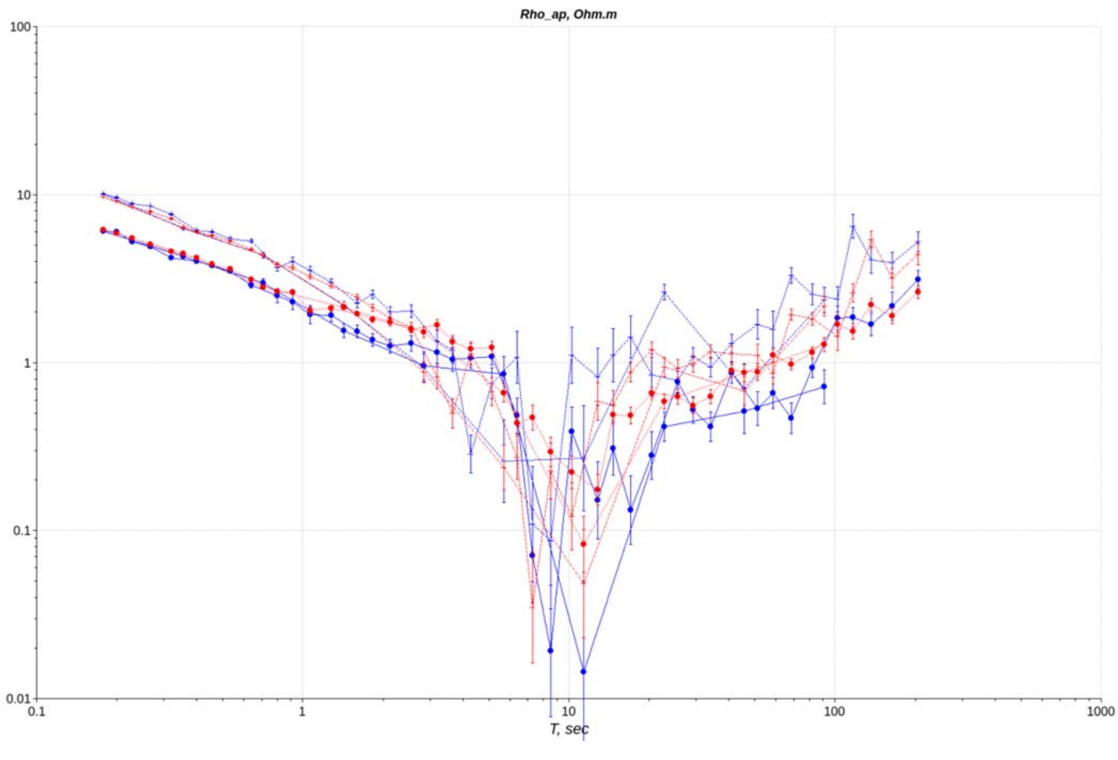

Figure A2.1. Comparison between single station and local remote reference estimation of apparent resistivities in x- and y-directions for station 25 using station 26 as a reference. Circles denote xy and crosses denote yx components of the apparent resistivity.
20 Hz sampling rate: Red=single station; Blue=reference station.

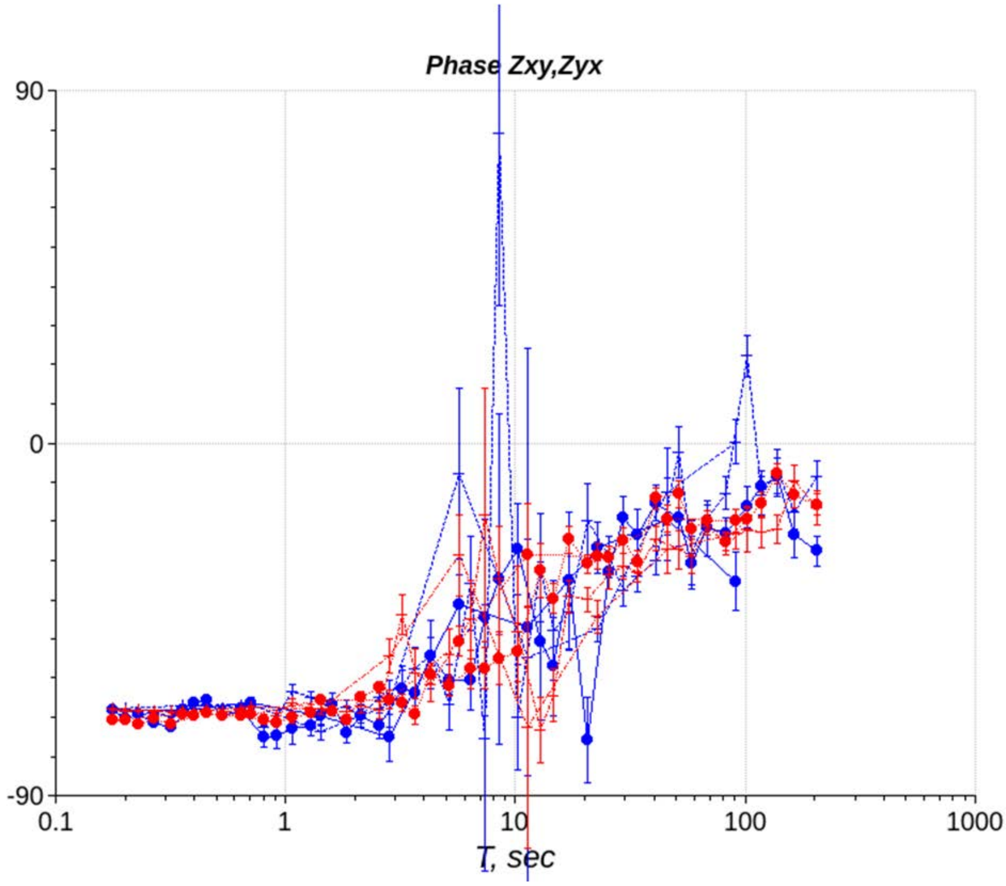

Figure A2.1. Comparison between single station and local remote reference estimation of phases in x- and y-directions for station 25 using station 26 as a reference. Circles denote xy and crosses denote yx components of the apparent resistivity.
20 Hz sampling rate: Red=single station; Blue=reference station.

4. Geology and information from seismics

An overview of the deep structures and the development of the sedimentary basins in Denmark can be found in Vejbæk (1997). Other key references are Bertelsen (1980), Dornenbal & Stevenson (eds., 1997) and Lokhorst (ed., 1997). The latter two references contain GIS compilations of data in relation to the hydrocarbon potential of the Southern Permian Basin area. Figures 4.1 and 4.2 show the depth to the top of the Chalk Group and the depth to the pre-Zechstein formations respectively within the Danish area. Figure 4.3 shows the rocks immediately below the pre-Zechstein surface and location of salt pillows and salt diapirs. The survey area (marked by rectangle in grey colour in Figures 4.2 and 4.3 is located on the Baltica plate east of the Caledonian Deformation Front as documented by the deep seismic MONA LISA project (see Abramovitz *et al.* 2008).

The survey area has previously been subject to intensive reflection seismic investigations and several deep (2–3 km) wells are located within the survey area. The Løgumkloster-1 well was drilled in 1980 (Dansk Boreselskab A/S, 1981) and hydrocarbons were encountered in a Zechstein carbonate sequence (Z2) at a depth of 2423–2451 m. Løgumkloster-1 well was drilled into pre-Zechstein metamorphic rocks a depth of 2724 m. The Løgumkloster structure is mapped as an east-west elongated closure, on the base of the Z2-salt which is interpreted conformable with the top of the Z2 carbonate. Maver (1995a, 1995b) used seismic data to map lateral variations in depth to the Z2 salt and porosity of Zechstein carbonate layers (Figure 4.4a,b). Clemmensen (1985) and Olsen (1987) provide interpretations of Triassic sequences observed in Løgumkloster wells situated within the northern part of the survey area.

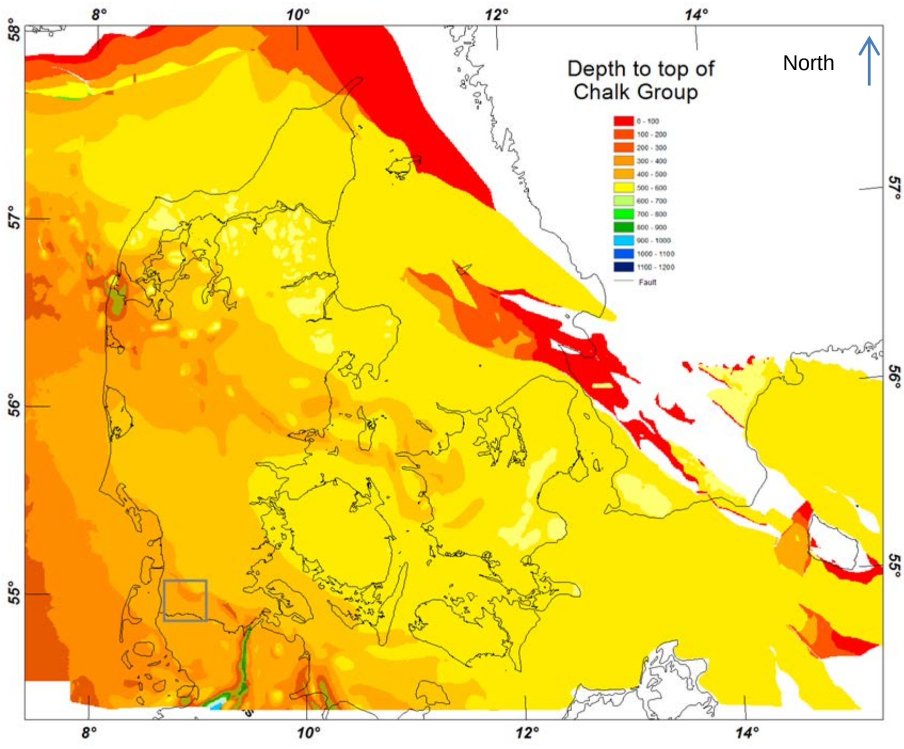

Figure 4.1. *Map to top Chalk Group. The rectangle in grey colour at latitude 55˚N marks the location corresponding to the map frame of the detailed maps in this report.*

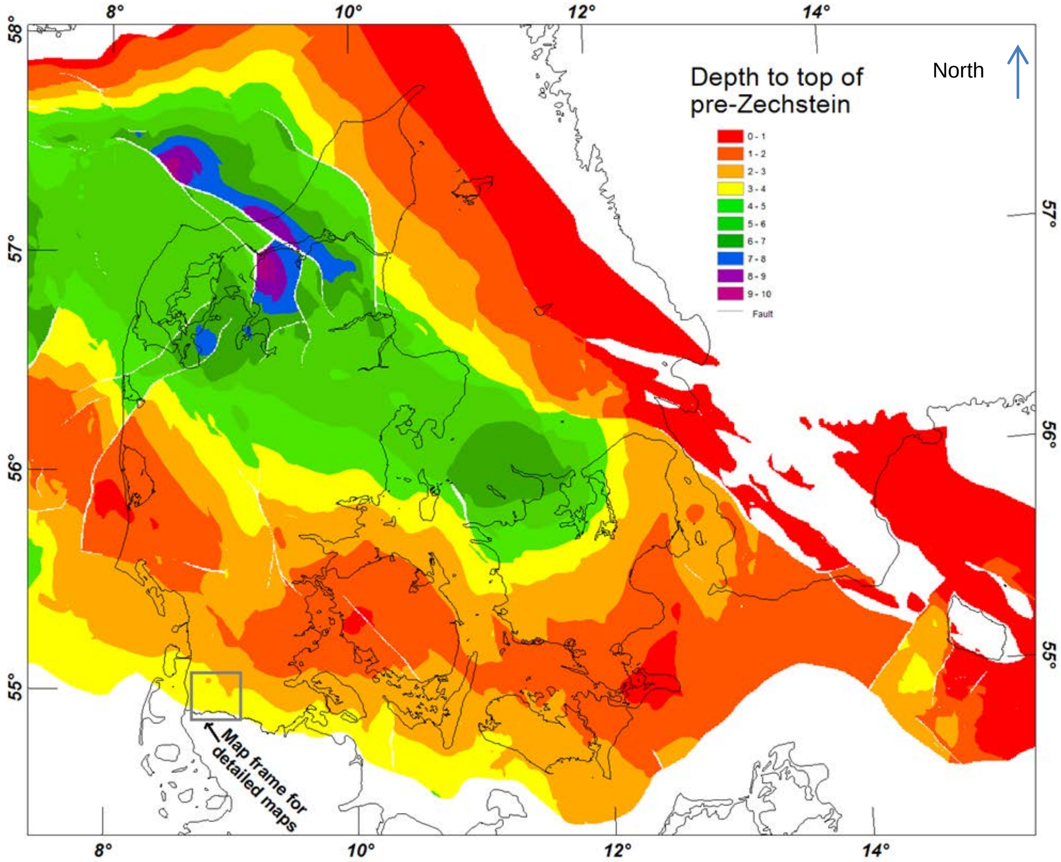

Figure 4.2. *Map to top of pre-Zechstein formations. The rectangle in grey colour at latitude 55˚N marks the location corresponding to the map frame of the detailed maps in this report.*

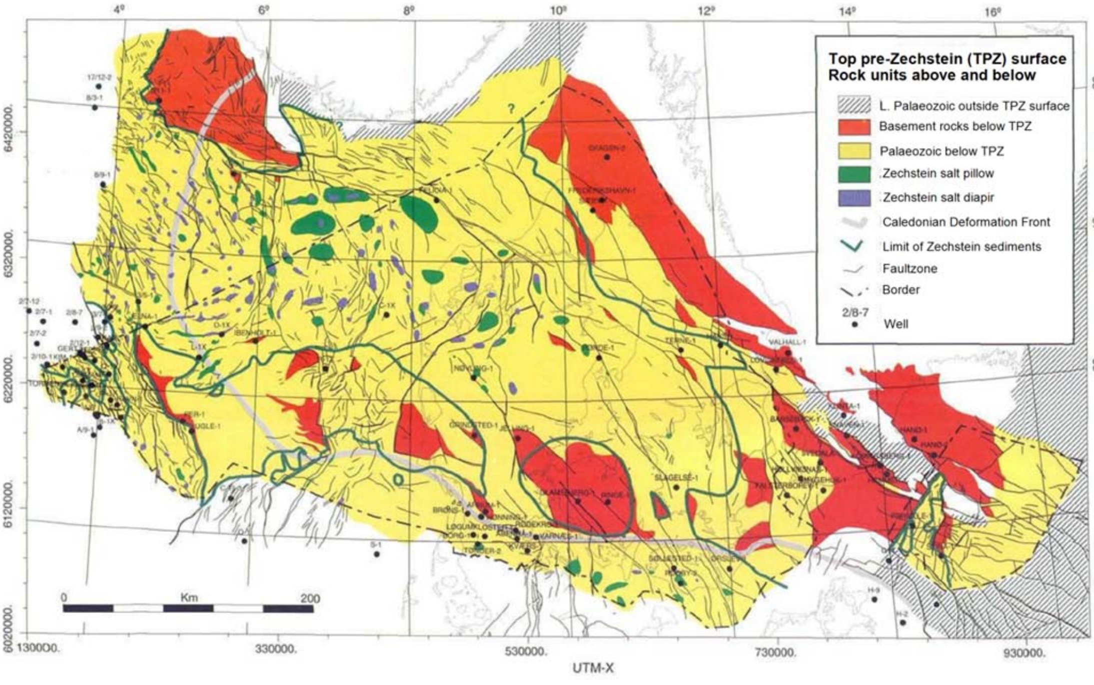

Figure 4.3. *Location of rock units with reference to the pre-Zechstein surface (from Vejbæk, 1997).*

(a)

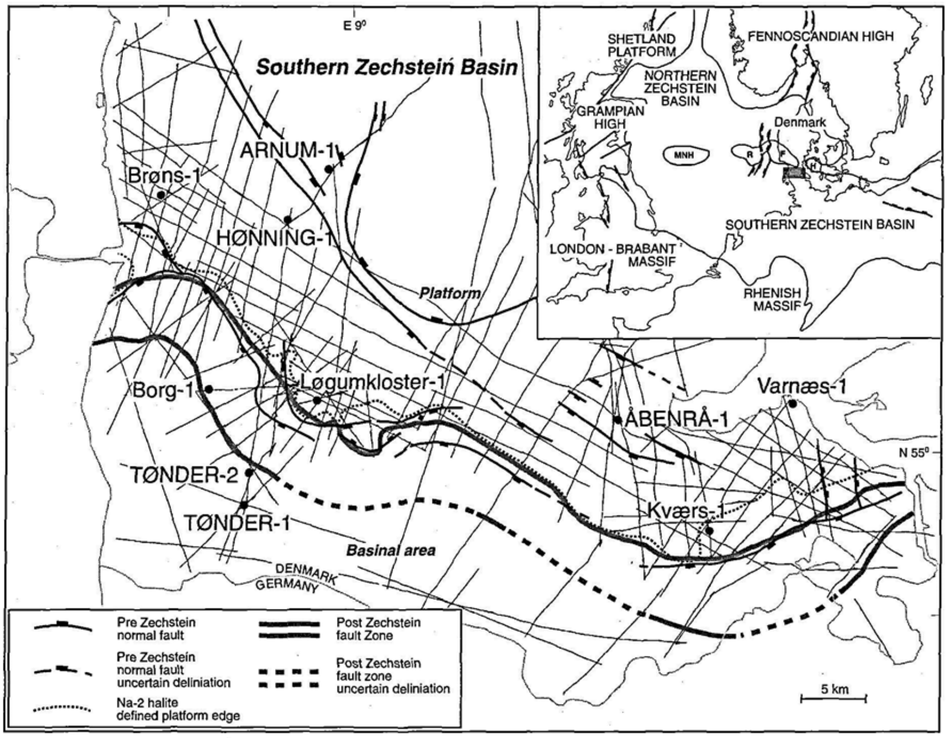

(b)

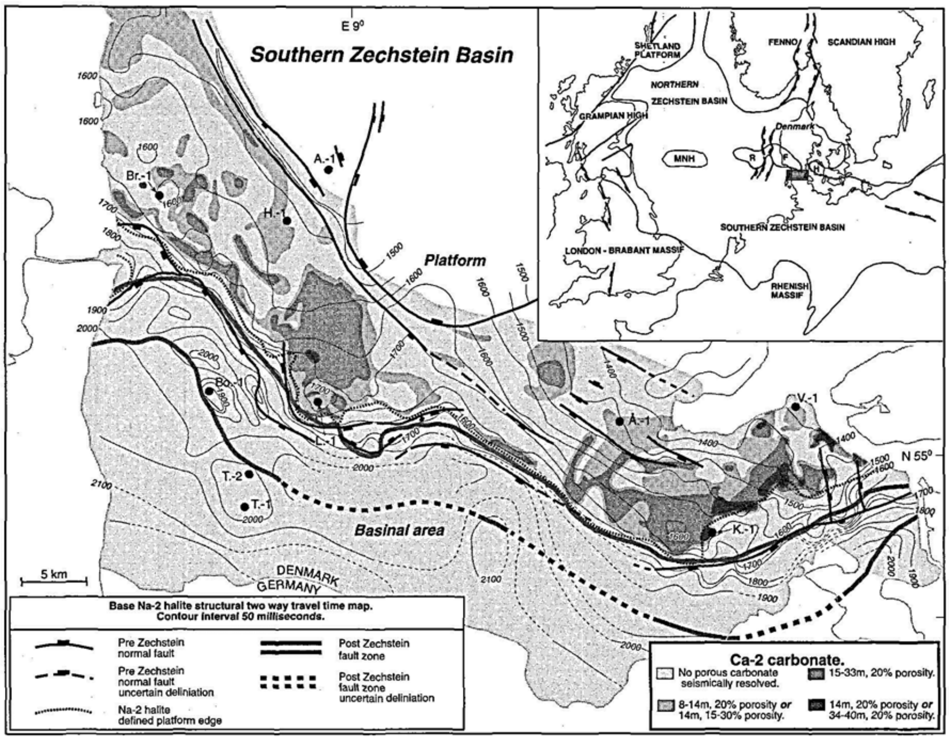

Figure 4.4. *(a) Seismic lines interpreted by Maver (1995a) and major structural elements in southern Jutland. (b) Distribution of Zechstein Carbonates derived from interpretation of seismic data and well logs. Note the salt pillow located at the Tønder-1 and Tønder-2 (T1 and T2) wells.*

5. Data and models

This chapter contains an introduction to data and models from the area of investigation. Maps are provided that show the 3D model obtained from inversion of the MT data. Other types of published data are shown that may be integrated in the interpretation of the MT data in future work. Considerable amounts of seismic data are in the archives at GEUS. A GIS compilation of these seismic data is on-going and expected to be released in 2013 in relation to a project on geothermal energy.

5.1 MT

In total 42 MT stations were measured at locations shown in Figure 5.1. The same map frame is used for the succeeding displays of data. The frequency content recorded is from 700 Hz to approximately 10^{-3} Hz; i.e. a part of the audio (AMT) frequency band (>1 Hz) is included. The average station spacing is 2.5 km, but considerable deviations from this average and a regular grid had to be made during the planning of the survey in order to avoid known potential electromagnetic noise sources. Other noise sources were encountered during the field work. In particular it was difficult to avoid noise signal from electrical fences operated by farmers in the survey area. MT tensor estimates and tipper functions from some of the MT stations were found to be of poor quality due to external noise, and they are excluded in the modelling conductivities based on the MT data (see Pedersen and Shan (2012; enclosure) on modelling). Nevertheless, it was possible to obtain data of sufficient high quality for the majority of the MT stations, which can be utilised in interpretations. A single MT station and a deep DC geo-electric sounding adjacent to the survey area (see Figure 5.1 for locations) are reported by Nissen (1982). Data from this thesis should be included in further work. A 1D interpretation of the MT data by Nissen (1982) gave depths to the basement (Zechstein?) of 2.2 km (based N-S apparent resistivity and phases) and 1.3 km (E-W apparent resistivity and phases).

Details concerning data processing and data inversion can be found in Pedersen and Shan (2012; enclosure). In the following, we only display and discuss the main results; i.e. the 3D model derived from inversion of the data. Figures 5.2 and 5.3 show horizontal sections through the 3D resistivity model at depths of 10 m, 200 m, 500m, 1000 m, 2000 m, 3000 m, 4500 m and 6000 m.

In short the results of the modelling can be classified by three domains: (1) an upper resistive domain of 400 m thickness underlain by (2) a very conductive domain extending down to about 3000 m followed by a (3) more resistive domain with gradually increasing resistivity. A tentative interpretation of these three domains is provided in the section below with information on deep wells.

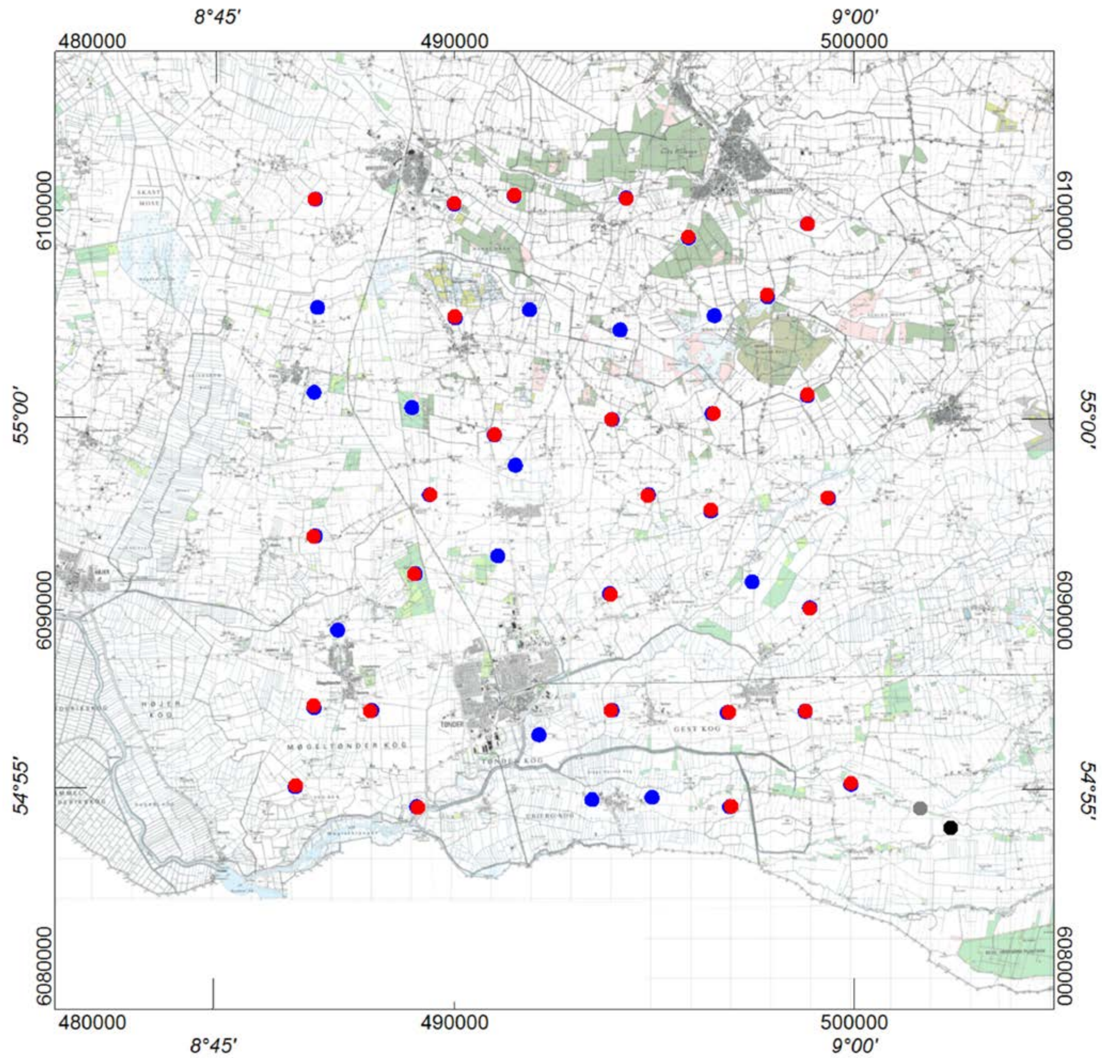

Figure 5.1. *Location of the 42 MT stations measured in this project. The same map frame is used for presentations of data below. The red dots mark MT stations included in the modelling, whereas MT stations marked with blue dots were too noisy for inclusion in the modelling. The MT station and DC geoelectric sounding by Nissen (1982) are shown by the black and grey dot respectively.*

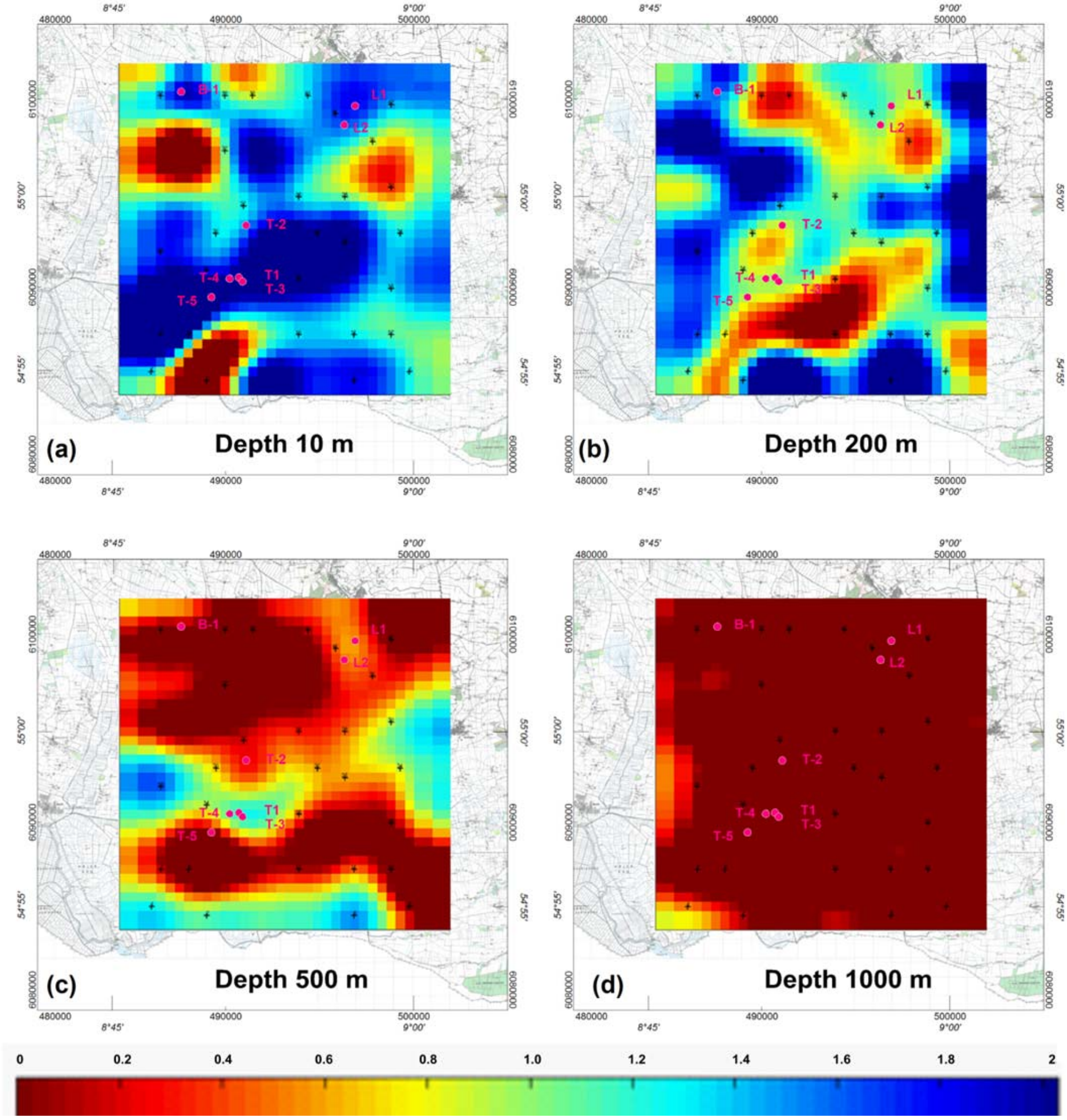

Figure 5.2 *Four horizontal sections at depths of (a) 10 m, (b) 200 mm, (c) 500 m and (d) 1000 m of the 3D resistivity model. Locations of deep wells (circles in red colour) Tønder 1-5; Borg-1 and Løgumkloster 1 & 2 are shown.*

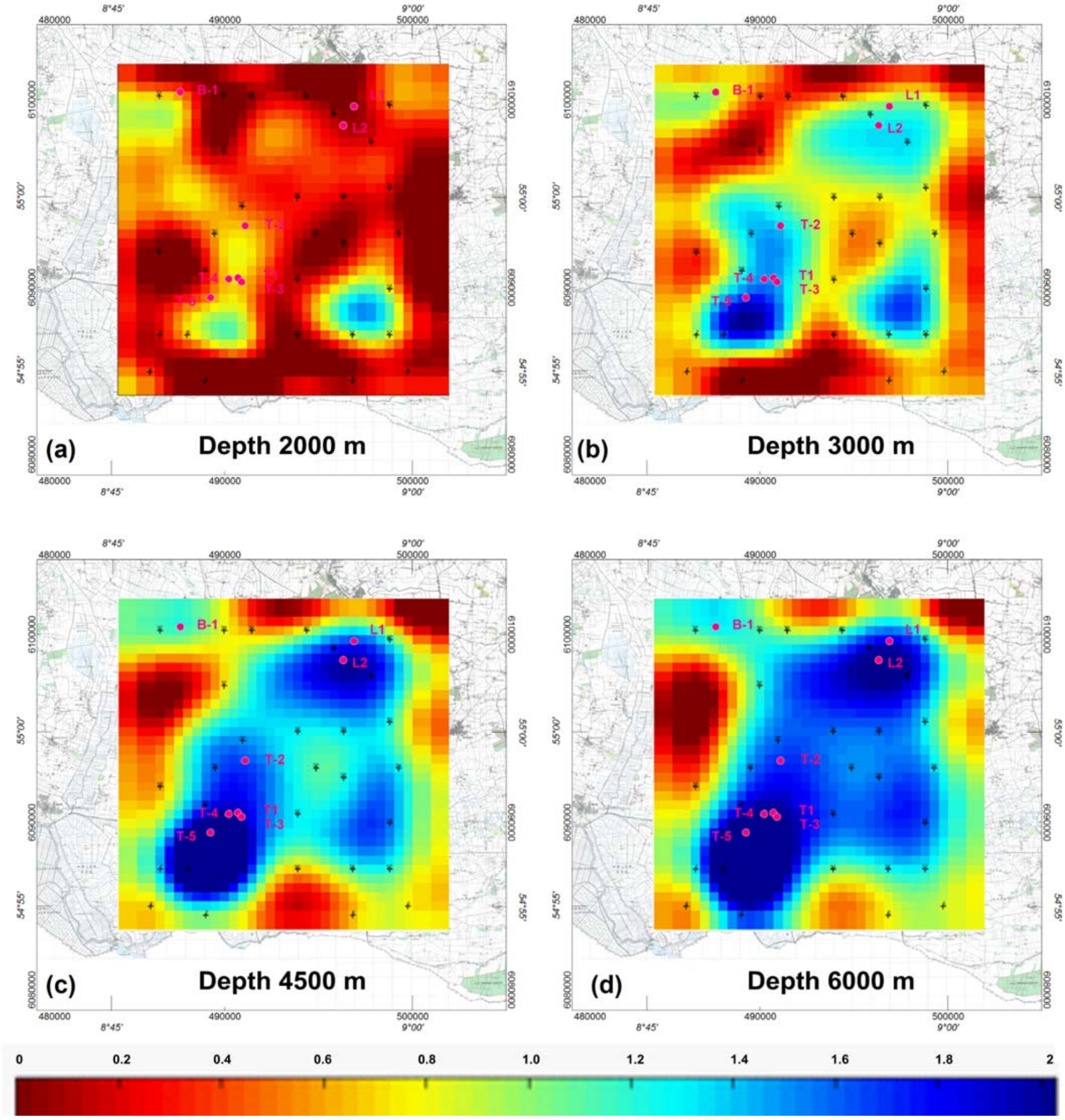

Figure 5.3. *Four horizontal sections at depths of (a) 2000 m, (b) 3000 mm, (c) 4500 m and (d) 6000 m of the 3D resistivity model. Locations of deep wells (circles in red colour) Tønder 1-5; Borg-1 and Løgumkloster 1 & 2 are shown.*

5.2 Wells and logging

Eight deep wells are located within the survey area. A summary is provided in a report by GEUS (1997). Their locations are marked in Figures 5.4 on a subset of the map by Maver (1995a) showing two-way travel times to the Z2 salt. The wells are

- Borg-1
- Løgumkloster-1
- Løgumkloster-2
- TØNDER No 1

- TØNDER No 2
- Tønder No 3
- ØSTERBY TØNDER No 4
- TØNDER No 5

Tables 1-8 contain depth to the chronostratigraphic units encountered for the eight wells. The information from the wells and the seismic interpretation show considerable variations in depth to the stratigraphic layers. The variations are partly due to the development of salt pillows and partly to faults (see Figures 4.3 and 4.4). Inspection of the horizontal sections in Figures 5.2 and 5.3 reveals that the salt pillow below Tønder is mapped by the MT data as a resistive structure at a depth of 2000 m. Other resistive structures at depth are at the southern edge of the Løgumkloster structure and about 10 km south of the Løgumkloster-2 well. The latter resistive structure does not correlate well with the Z2 salt horizon mapped by Maver (1995a) in this area (see Figure 4.4). The lack of correlation may be due to lack of seismic data from this particular area. The resistive structure at the southern edge of the Løgumkloster structure is mapped at a depth of 3000 m; i.e. considerable deeper than the two other resistive structures. The depth to the resistive structure at Tønder is consistent with the occurrence of Permian rocks reported from the wells (Tables 4 and 5).

Resistivity logs from the wells are shown in Figure 5.5. A corresponding 100 samples median filtered version of the resistivities [Ωm] in $\log_{10}$ units are shown by the colour code. The type of log differs among the wells. The type of log with deepest penetrations has been chosen for the display in order to provide the best estimate of the sediment resistivities The most shallow (1540 m; see Table 1) occurrence of the Zechstein layer is marked by high resistivities (>2000 Ωm) in the Borg-1 well. The Borg-1 well is furthermore characterised by thin layers with alternating high and low resistivities within the lower part of the Zechstein unit. The 3D resistivity model does not show the high resistivities corresponding to the upper part of the Zechstein unit, except for a weak increase in resistivity south of the well in the Z=2000 m and Z=3000 m sections. In general, resistive layers are transparent with respect to MT data unless the thickness is very large. Conductive sediments below or in sections within the lower part of the Zechstein layer may here be the reason for fairly low apparent resistivities (10 Ωm) at periods of 100s. The smoothness constraint that is built into the inversion procedure may therefore have forced the model to give unrealistic low resistivities in the area around the Borg-1 well.

The classification of the resistivity model in three domains roughly corresponds to (see Figure 5.6) the (1) Post Chalk Group as the upper 400 m resistive domain, (2) the Chalk Group, L. Cretaceous and upper part of the Triasic units representing the "good conductor" underlain by a more siliciclastic Triassic unit with intermediate conductivity. The lower resistive domain is interpreted as representing Zechstein. The different horizon slices from Z= 2000 m and deeper furthermore illustrates that the sub-surface is more complex and that significant post-depositional halokinesis has taken place, as piercings of several high resistivity salt pillows (?) penetrate the good conductive sediments (low resistivity), (Z=3000 m). In conclusion, without taking into account for the depth uncertainties, it seems that the MT method can separate large-scale lithology variations and help to identify good conductors. Mapping of good conductors in relation to hydrocarbon prospectivity mapping is linked to the presence of alteration zones surrounding reservoirs. The increase in conductivity is mainly a result of disseminated pyrite. The MT results are however not conclusive and can only serve as a guide to areas of interest.

Inclusion of resistivity data from the wells as constraints in the inversion of the MT data should be utilised in future work. In particular it is important to verify that the MT data are consistent with information from the logs; i.e. if it is possible to obtain an acceptable data fit when using well log data as constraints.

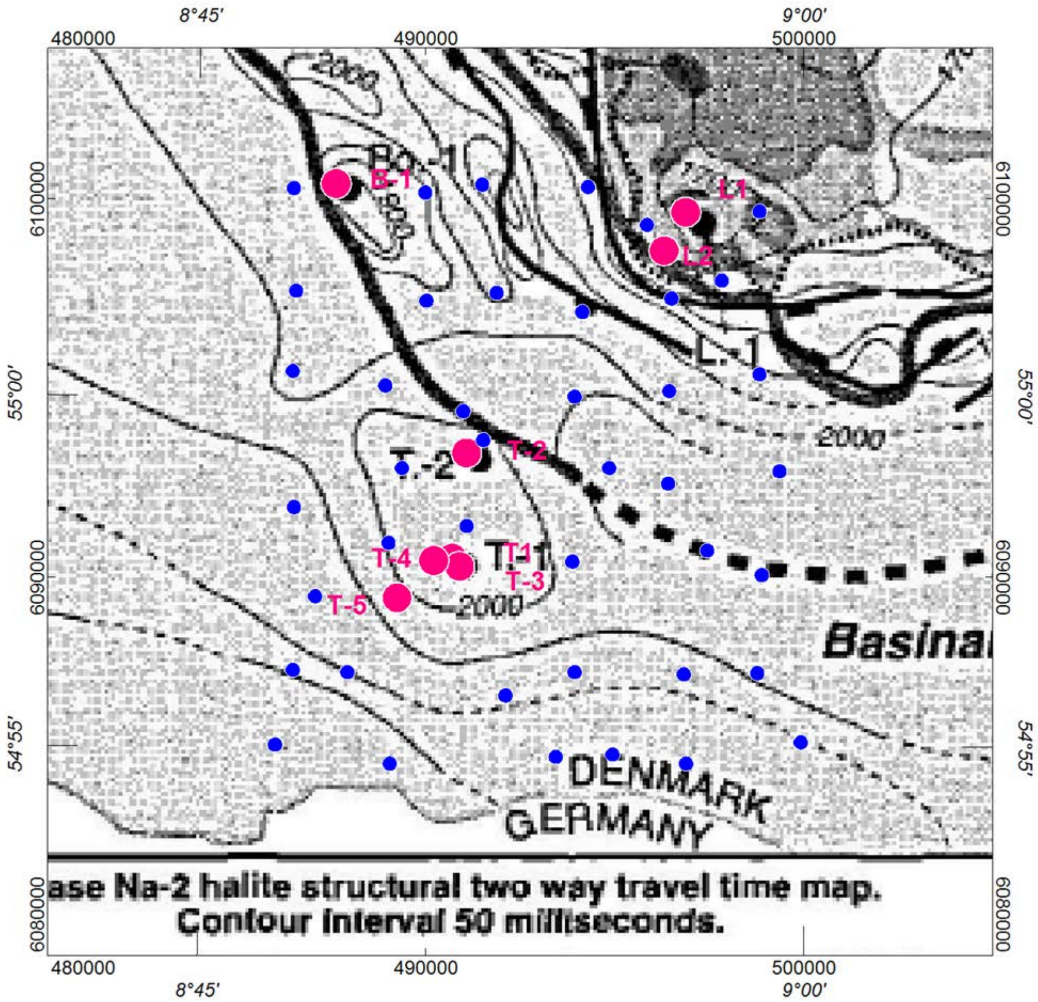

Figure 5.4. *Map showing the locations of deep wells (circles in red colour, Tønder 1-5; Borg-1 and Løgumkloster 1 & 2) in the survey area and the locations of MT stations (circles in blue colour). The background image within the Danish area is from Maver (1995a) which shows the two-way travel time to the Z-2 halite structure (100 ms isolines) and porosity interpretations of the Z2 layer (see Figure 4.4).*

Table 1. *Chronostratigraphy for Borg-1 well*

Top	Bottom	Unit
6.0 m.	44.0 m.	Quaternary
44.0 m.	714.0 m.	Tertiary
714.0 m.	1,354.0 m.	Cretaceous

1,354.0 m.	1,540.0 m.	Triassic
1,540.0 m.	3,019.0 m.	Permian
3,019.0 m.	3,072.0 m.	Carboniferous

Table 2. *Chronostratigraphy for Løgumkloster-1 well*

Top	Bottom	Unit
6.0 m.	70.0 m.	Quaternary
70.0 m.	430.0 m.	Tertiary
430.0 m.	1,028.0 m.	Cretaceous
1,028.0 m.	2,178.0 m.	Triassic
2,178.0 m.	2,709.0 m.	Permian
2,709.0 m.	2,724.0 m.	Ordovician

Table 3. *Chronostratigraphy for Løgumkloster-2 well*

Top	Bottom	Unit
7.0 m.	81.0 m.	Quaternary
81.0 m.	457.0 m.	Tertiary
457.0 m.	1,034.0 m.	Cretaceous
1,034.0 m.	2,117.0 m.	Triassic
2,117.0 m.	2,786.0 m.	Permian

Table 4. *Chronostratigraphy forTønder-1 well*

Top	Bottom	Unit
5.0 m	50.0 m	Quaternary
50.0 m	428.0 m	Tertiary
428.0 m	976.0 m	Cretaceous
976.0 m	2,154.0 m	Triassic
2,154.0 m	3,124.0 m	Permian

Table 5. *Chronostratigraphy forTønder-2 well*

Top	Bottom	Unit
4.0 m	52.0 m	Quaternary
52.0 m	488.0 m	Tertiary
488.0 m	1,087.0 m	Cretaceous
1,087.0 m	2,437.0 m	Triassic
2,437.0 m	3,201.0 m	Permian

Table 6. *Chronostratigraphy forTønder-3 well*

Top	Bottom	Unit
6.0 m.	425.0 m.	Tertiary
425.0 m.	854.0 m.	Cretaceous
854.0 m.	977.0 m.	Cretaceous
977.0 m.	1,840.0 m.	Triassic

Table 7. *Chronostratigraphy forTønder-4 well*

	Bottom	Unit
8.0 m.	429.0 m.	Tertiary
429.0 m.	974.0 m.	Cretaceous
974.0 m.	1,870.0 m.	Triassic

Table 8. *Chronostratigraphy forTønder-5 well*

Top	Bottom	Unit
8.0 m.	432.0 m.	Tertiary
432.0 m.	982.0 m.	Cretaceous
982.0 m.	1,915.0 m.	Triassic

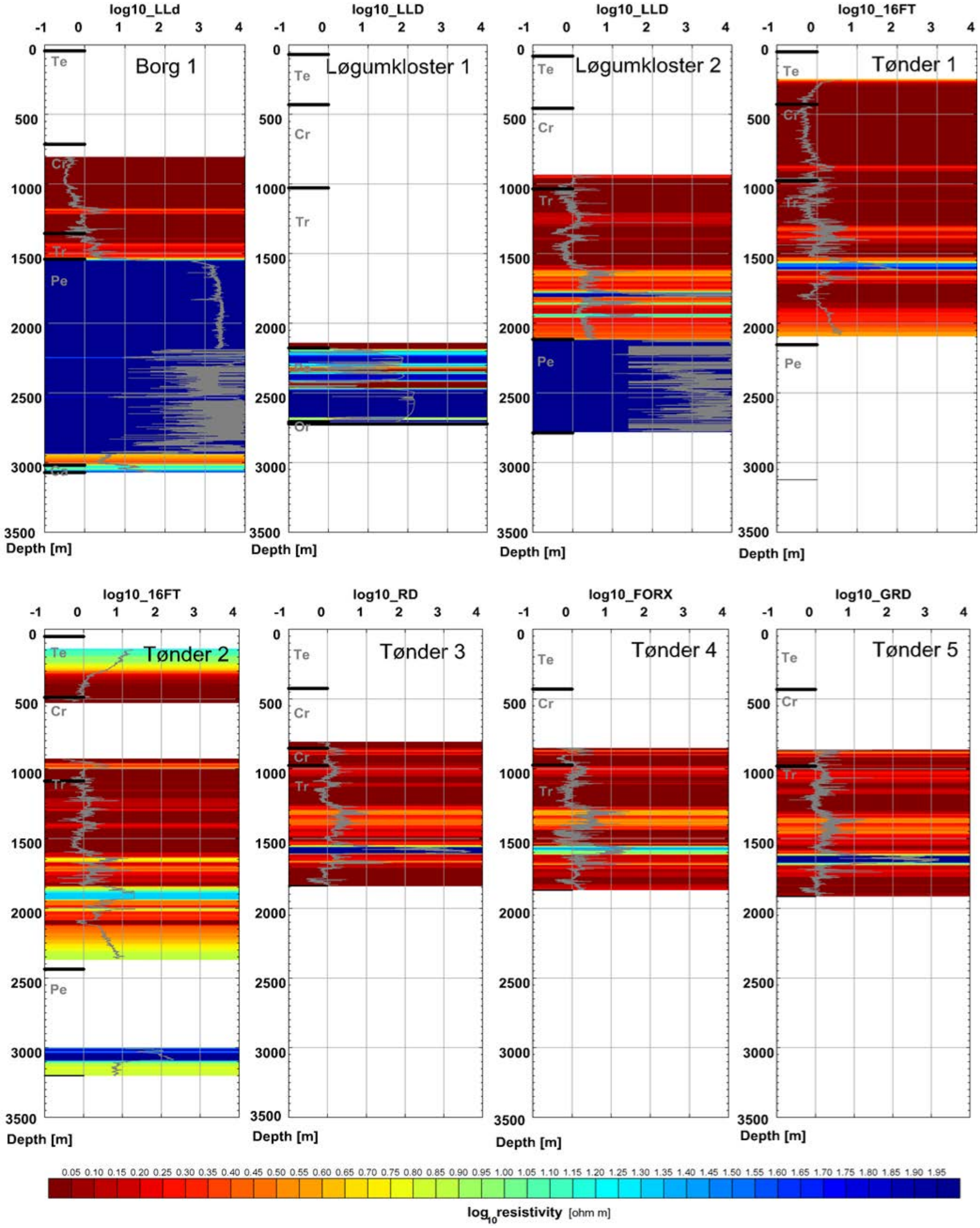

Figure 5.5. *Resistivity logs from wells Borg-1, Løgumkloster-1, Løgumkloster-2 and Tønder 1-5. Note that log type differs among the wells. Resistivities [Ωm] are shown in log_{10} units. Lines in grey colour correspond to measured values and colours correspond to 100 sample median filtered log_{10} data. Chronostratigraphic divisions are shown by thick black lines and locations of well bottoms are shown by thin black lines.*

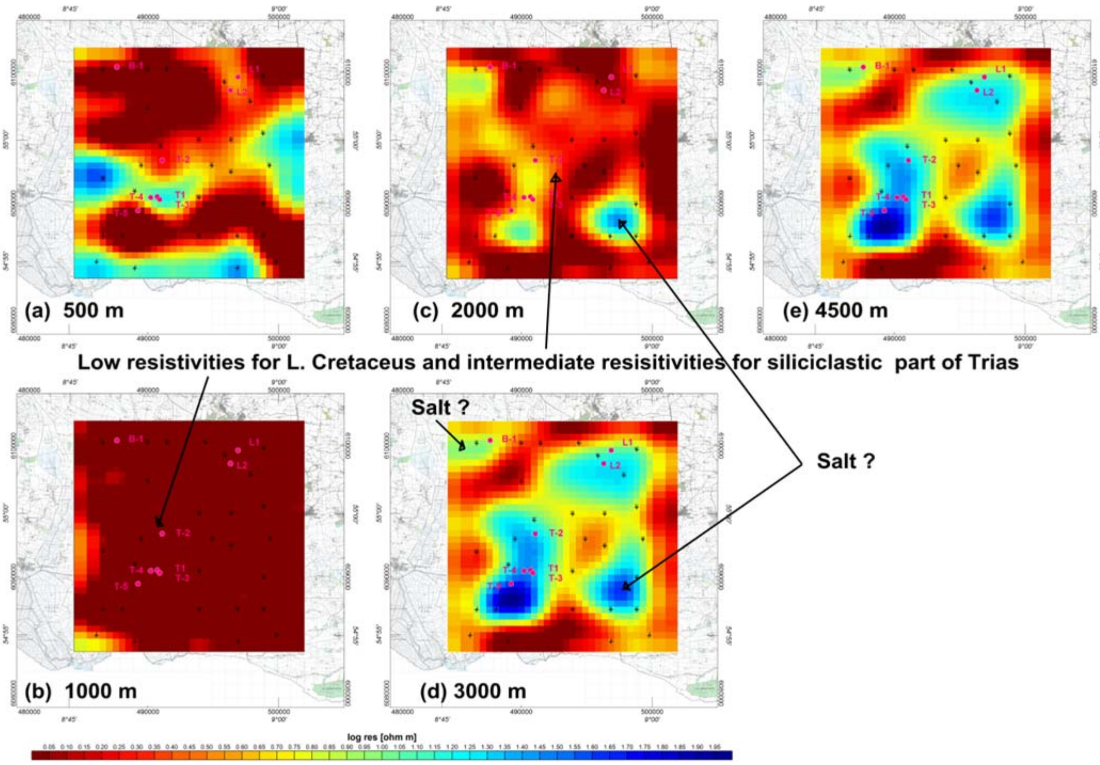

Figure 5.6. *Tentative interpretation of 3D resistivity model.*

5.3 SkyTEM survey

An airborne electromagnetic survey (SkyTEM system; see Figure 5.7) covers almost the entire area surveyed for this report. Data and interpretations from the airborne electromagnetic survey are described in Jørgensen *et al.* (2012). Figure 5.8 includes two horizontal sections obtained from the model based on the SkyTEM survey and two sections at approximately the same depth from the 3D conductivity model derived from the MT data. The large station separation of the MT survey does not allow a detailed mapping of lateral resistivity variations. Nevertheless, the resistivity sections derived from the two types of geophysical data show consistency with respect to structural features and resistivity values.

Although the investigation depth of the airborne survey is limited to the upper 250 m approximately, the high resolution laterally as well as with depth may be utilised in joint inversions with the acquired MT data and subsequent interpretations, constraining the modelling of the deeper sections.

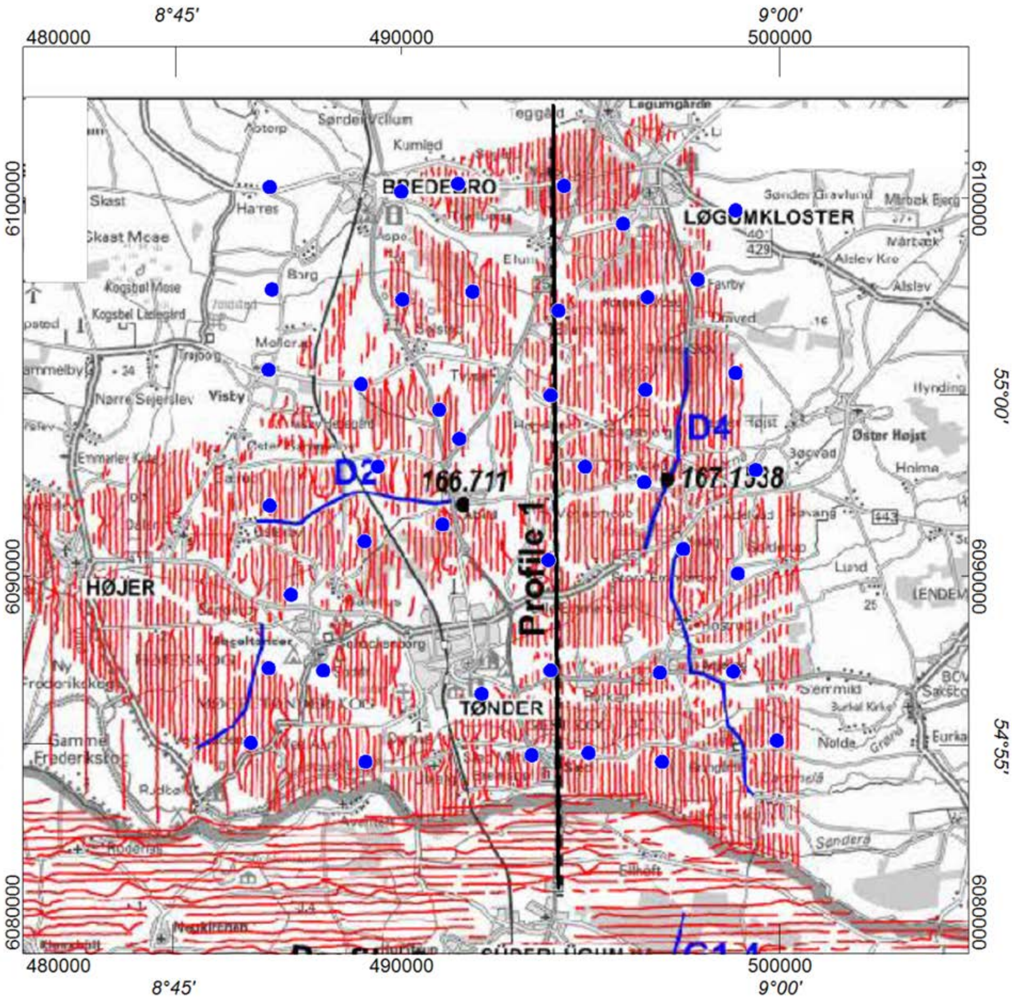

Figure 5.7. *Location of SkyTEM profiles (red lines) within the area of investigation with MT data. The circles in blue mark the location of MT station (map from Jørgensen et al. 2012)*

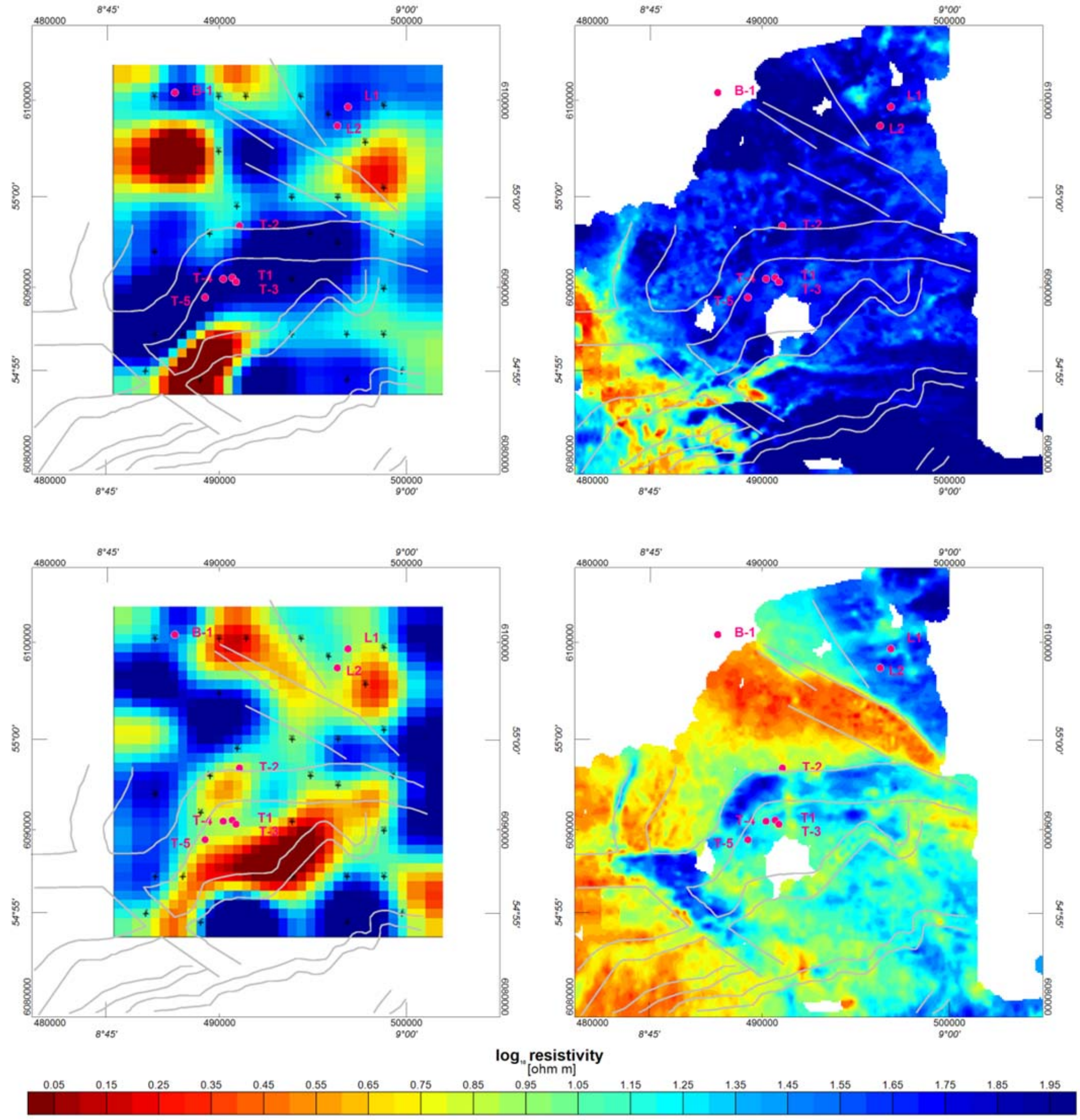

Figure 5.8. *Horizontal sections from the 3D MT model and the SkyTEM model. Lines drawings are structural elements interpreted by Jørgensen et al. (2002).*

6. Concluding remarks

The 3D inversion method used here search for smooth models that fits the data within the data errors. The basic argument for using this type of model is that any short wavelength variations must reflect real resistivity variations. The degree of smoothness provides a rough measure of the resolution of the method for the particular area and data set. The 3D model includes a number of features of which some are consistent with the other data but other features are not readily explained. Interpretation of 3D data sets (surface coverage instead of profiles) and the use of 3D inversion have become possible only very recently, and much more work is required to exploit achievements and limitation of this new opportunity. Constraints from well logs and other types of information should be attempted. The inclusion of constraints in the 3D inversion can also be utilized for investigation of upper and lower bounds on resistivities. Such an analysis (essentially a non-linear most squares inversion; see Jackson (1976)) is going to be extremely time-demanding, because each solution must be found iteratively with inclusion of a full non-linear 3D least-squares inversion.

Interpretation of induced polarisation effects in MT data has been reported from a case study in China (He *et al.* 2010). Inclusion of induced polarisation effects in the 3D inversion has not been possible for this report, but should be considered for future work.

The purpose of this presentation of the MT data together with other data types is primarily meant to provide information and directions for possible further work. A fuller interpretation in relation to hydrocarbon prospectivity is premature. If this had been the goal, considerable more efforts to integrate with other types of data would have been required to fully utilise the MT data and evaluate these in relation to hydrocarbon exploration purposes. The high resolution model of the upper 250 m based on the SkyTEM data could provide valuable information if used as a constraint in the inversion of the MT data. In particular, constraints from seismic data would be very helpful. However, the scenario for the ALTKUL project asks for an evaluation of alternative non-seismic methods and in that scenario the question would be if the MT data, supported by other non-seismic data, could replace seismics as the basis for a go/no go decision for further exploration activities. Results obtained from integration of MT data with seismic data in the case of the Tønder area in future investigations must viewed with this in mind.

7. Acknowledgements

The authors would like to thank DONG E&P A/S and Nordsøfonden for funding this study.

The contributions by Soroor Mohammadi and Mahboubeh Montazeri to the field work are highly appreciated.

Thanks go to farmers and others in the Tønder area who gave their permission for the measurements. Their support and kind assistance are highly appreciated.

8. References

Abramovitz, T., Thybo, H., MONA LISA Working Group, 1998. Seismic structure across the Caledonian deformation front along MONA LISA profile 1 in the southeastern North Sea. Tectonophysics, **288** (1–4), 153–176.

Bertelsen, F. (1980): Lithostratigraphy and depositional history of the Danish Triassic. Danmarks Geologiske Undersøgelse Serie B., **4**, 59 pp.

Cagniard, L. 1953: Basic theory of the magnetotellurics method of geophysical prospecting. Geophysics **18**, 605–635.

Chave, A.D. & Jones, A.G. 2012: The magnetotellurics method – Theory and Practice. Cambridge University Press. ISBN 978-0-521-81927-5.

Clemmensen, L.B. (1985): Desert sand plain and sabkha deposits from the Bunter Sandstone Formation (L. Triassic) at the northern margin of the German Basin. Geologische Rundschau, **74** (3), pp. 519–536.

Dansk Boreselskab A/S, 1981: Løgumkloster-1, Completion Report. In Archives of the Geological Survey of Denmark and Greenland, GEUS Report File no. 7281.

GEUS, 1997:Wll data summary sheets Volume 27. Released wells from southern Jylland. . Danmark og Grønlands Geologiske Undersøgelse Rapport, **25**, 152 pp.

He, Z., Hu, Z., Luo, W. & Wang, C. 2010: Mapping reservoirs based on resistivity and induced polarization derived from continuous 3D magnetotelluric profiling: Case study from Qaidam basin, China. Geophysics **75**(1), January-February; B25–B33.

Jackson, D.D. 1976: Most squares inversion. Journal of Geophysical Research, **81**, 5, p. 1027.

Jørgensen, F., Scheer, W. Thomsen, S., Sonnenborg, T.O, Hinsby, K., Wiederhold, H., Schamper, C., Burschil, T., Roth, B., Kirsch, R: & Auken, E. 2012:Transboundary geophysical mapping of geological elements and salinity distribution critical for the assessment of future sea water intrusion in response to sea level rise. Hydrol. Earth Syst. Sci., **16**, 1845–1862

Li, X. & Pedersen, L. B. 1984: Controlled source tensor magnetotellurics. Geophysics **56**(9), 1456–1461.

Maver, K.G. 1995a: Seismically detected porous Zechstein carbonates in Southern Jutland, Denmark, Bulletin of the Geological Society of Denmark. Vol. **42**, pp. 34–46. Copenhagen.

Maver, K.G. 1995b: Porosity evaluation of seismically-resolved Zechstein Carbonate layers. Løgumkloster- 1 Well, Denmark. Journal of Petroleum Geology, **18** (3), pp. 329–344, July 1995.

Nissen, J. 1982: Magnetotelluriske sonderinger i Jylland, 1981: Speciale afhandling ved Laboratoriet for geofysik, Aarhus Universitet, 1982.

Olsen, H. (1987): Ancient ephemeral stream deposits: a local terminal fan model from the Bunter Sandstone Formation (L. Triassic) in the Tønder-3, -4 and –5 wells, Denmark. In: Frostick, L. & Reid, I. (eds.): Desert Sediments: Ancient and Modern. Geological Society Special Publication, **55**, pp. 69–86.

Rasmussen, T. M. & Thorning, L. 2012: Review of selected non-seismic methods for onshore hydrocarbon exploration in Denmark. ALTKUL Project Report Part 1. Danmark og Grønlands Geologiske Undersøgelse Rapport, **88**, 74 pp., 1 appendix.

Tikhonov, A.N. 1950: On determination of electric characteristics of deep layers of the earth's crust. Dokl. Acad. Nauk SSSR **151**, 295–297.

Tikhonov, A.N. 1965: Mathematical basis of the theory of electromagnetic sounding: USSR Comp., Math. & Phys., 201–211.